

Model of response spectrum and modal interaction in coupled nanomechanical resonators

J. Dorignac¹, A. Gaidarzhy¹, P. Mohanty²

¹ *College of Engineering, Boston University, Boston MA 02215*

² *Department of Physics, Boston University, Boston MA 02215*

(Dated: November 21, 2021)

We develop a simple *continuum* model to analyze the vibrational modes of a nanomechanical multi-element structure. In this model, arrays of sub-micron cantilevers located symmetrically on both sides of the central clamped-clamped nanobeam are replaced by a continuum. In this approach, the punctual shear forces exerted by the cantilevers on the central beam are smoothed out and the equations of motion of the structure become exactly solvable. Our analytical results capture the main features of the vibrational modes observed both numerically and experimentally. Furthermore, using a perturbative approach to treat the nonlinear dynamics of the structure, we establish its frequency-amplitude response and analyze the mechanism of anharmonic coupling between two specific widely spaced modes of the resonator.

PACS numbers: 03.65.Ta, 62.25.-g, 62.30.+d, 62.40.+i

I. INTRODUCTION

Nanomechanical resonators have been used to investigate fundamental physics problems in a wide range of research areas. These include quantum measurement and quantum computation [1, 2, 3, 4, 5], ultra-sensitive force and mass detection [6], single spin detection [7], gravitational wave detection [4, 5] and other fundamental phenomena [8, 9, 10, 11]. The central reason for the increasing interest and activity in nanomechanical systems for quantum studies is straightforward: fast dynamics of nanomechanical systems enable the investigation of the yet-unexplored corner of the parameter space where ultra-high frequency resonance modes cooled to near-zero temperatures are expected to manifest quantum mechanical corrections to the classical motion [12, 13, 14].

Likewise, from a technological standpoint, compact size, robustness, and high frequencies of nanomechanical resonators have resulted in numerous proposals for applications where technologies involving nanomechanical systems can offer alternative solutions to the existing electronic circuits and off-chip devices: frequency selective oscillators [15], passive filters [16], memory elements [17] and spintronics devices [18].

Despite the broad areas of interest in nanomechanical systems, comprehensive studies of elasticity and mechanics of nanomechanical structures are yet to be done beyond the simple single-element structures such as cantilevers and clamped beams. The main difficulty has been the extension of elasticity theory to multi-element structures for closed-form analytical solutions. As described in the following, most of the eventual applications of nanomechanical systems will include complex structure design. Therefore, analytical understanding of resonant modes and other dynamical aspects such as nonlinear mode coupling in complex multi-element structures will be of tremendous importance. Here, we briefly describe a few areas of interest in which nanomechanical structures in the gigahertz range will play a key role.

A. Entry into the Quantum Regime

Experimental access to the quantum realm is *crudely* defined as the regime in which the quantum of energy hf in a resonant mode with frequency f is larger than the thermal energy $k_B T$ of the environment. The motivation behind this crude definition of the quantum regime is simple. The motion of a damped mechanical system can be described by a harmonic oscillator potential. In the quantum regime, the harmonic oscillator potential energy levels are discrete. In order to observe effects of discrete energy levels, smearing by thermal energy—due to finite temperature of the mechanical system—must be small compared to the energy level spacing, hf . The condition $hf \geq k_B T$ gives physically relevant parameters: a nanomechanical structure with a normal mode resonance frequency at 1 GHz will enter the quantum regime below a temperature $T \equiv (h/k_B)f = 48$ mK. Since typical dilution cryostats have a base temperature of 10 mK, nanomechanical structures with frequencies above 1 GHz can enable experimental access to the quantum regime. The experimental challenge is then to fabricate structures capable of high gigahertz-range resonance frequencies, and to measure them at low millikelvin-range temperatures. Since the resonance frequency increases with decreasing size of the system, one or many of the critical dimensions of the gigahertz-frequency oscillators must be in the sub-micron or nano scale.

B. Mesoscopic Elasticity: Multiscale Modeling

For large mechanical structures, continuum mechanics of elasticity theory provides the appropriate system response, both static and dynamic. As system size shrinks down to the submicron or nano scale, the elastic behavior starts to become atomistic rather than continuous, and it gives rise to a host of anomalous behaviors [19]. These include enhancement of influence of surface defects, novel dissipation mechanisms, reduction of the stiffness con-

stant, and statistical fluctuation effects. Nanomechanical resonators therefore need to be modeled by atomistic simulation in order to capture the essential aspects of their elastic properties arising due to mesoscopic size. However, atomistic simulation of these structures containing about 100 million atoms or more becomes computationally intensive. Further problems arise due to the existence of multiple length scales. Modeling of structures too small for continuum mechanics and too large for atomistic molecular dynamics simulation requires a proper understanding of the coupling of length scales.

For a comprehensive study of nanomechanical systems, the structures need to be properly characterized for their elastic behavior. Specifically, correlation of simulated modeshapes and experimentally-measured modes will require the knowledge of relevant static and dynamic parameters. Therefore, analytical studies of complex nanomechanical systems will not only provide a strong motivation for new approaches to model materials beyond the current limit of computing capacity, it will augment the ongoing work on the multiscale modeling of fracture dynamics and nanomaterials.

C. Nanomechanical Device Applications in the Gigahertz Range

The driving force behind MEMS (Micro-Electro-Mechanical Systems), of which NEMS (Nano-Electro-Mechanical Systems) or nanomechanics is the natural extension, has been the portfolio of MEMS applications in optical communication (routers, switches, repeaters), passive devices in cell-phone industry (filters, accelerometers, capacitors and inductors for integrated chip design), and sensor technologies in chemical, biomedical, and electrical solutions. Nanomechanical structures are faster (because of higher resonance frequencies), therefore the natural area of growth for these applications includes technologies for multi-function nanomechanical devices: ultra-sensitive force sensors for the detection of fundamental forces and biomolecular forces. The technologies needed for observing quantum effects will have obvious use in these and other gigahertz-range applications. In fact, the range of frequencies discussed in this paper matches with the frequency bands for communication in a number of consumer devices: Cellular (0.4 GHz, 0.85 GHz, 1.9 GHz), WiFi and Bluetooth (2.4 GHz), Satellite radio (~ 2.3 GHz), and GPS receivers (L1-L3: 1.2-1.6 GHz).

In basic research, hybrid nanomechanical devices in the gigahertz range can prove to be crucial in a number emerging fields. For example, there has been a recent proposal for spintronics based entirely on nanomechanical torque associated with the electron spin [18]. This device is an example of multi-function nanomechanical device, which, in the gigahertz range, can provide access to control and manipulation of electron spin at the spin coherence and spin relaxation time scales of nanoseconds.

Since the structure size is reduced for increasing res-

onant mode frequencies—and hence the operation speed of the device, it is possible that within a few years certain applications with nanomechanical devices will emerge which will have frequencies high enough so that at the relevant operating temperatures the nanomechanical element will be quantum mechanical. A specific application of gigahertz-range nanomechanical oscillators involves space communication devices (0.5-18 GHz). As passive devices, nanomechanical structures in certain space communication applications are expected to remain at low temperatures, perhaps near the quantum regime. This leads to the obvious realization that further shrinkage of micro- or nanomechanical systems with corresponding high gigahertz-range frequencies will inevitably require new paradigms.

D. Approaches to Gigahertz Resonance Frequencies

Central to many of the aforementioned applications of NEMS resonators is the attainment high natural frequencies of motion up to and beyond the 1-GHz mark. Among the various solutions proposed for achieving ultra-high frequencies in nanomechanical resonators such as the use of high stiffness materials [20, 21] and bulk mode geometries [22], our approach of coupling mechanical elements to enhance high order resonant modes of the resonator structure has been shown to offer a number of advantages for performance and detection ease [23]. The coupling of additional degrees of freedom to a 10- μm -long simple nanobeam structure can produce significant modification of the high order resonance spectrum, with enhanced amplitude and quality factors of selected vibration modes extending well beyond the 1 GHz frequency range.

E. Organization of the Paper

Here, we present two analytical models that yield closed-form solutions describing the dynamics of the coupled-beam resonator, dubbed the antenna structure. This structure is a prototype of a class of two-element structures that can be envisioned in specific applications. The continuum model allows for a clear comparison of the modal shapes and spectrum with full finite element analysis of the structure. We further investigate nonlinear modal coupling between widely spaced modes of the structure using perturbation theory techniques.

In Section II, we describe a discrete model of the antenna-like multi-element structure, and we obtain exact solution for the vibrational modes. In Section III, we extend this analysis to a continuum approximation where the periodic and punctual force densities are smoothed out. In this continuum model, we describe the frequency spectrum and the corresponding band structure. Specifically, we calculate fundamental and collective modes and we compare the results with finite element analysis. In Section IV, we consider a specific example of nonlinear

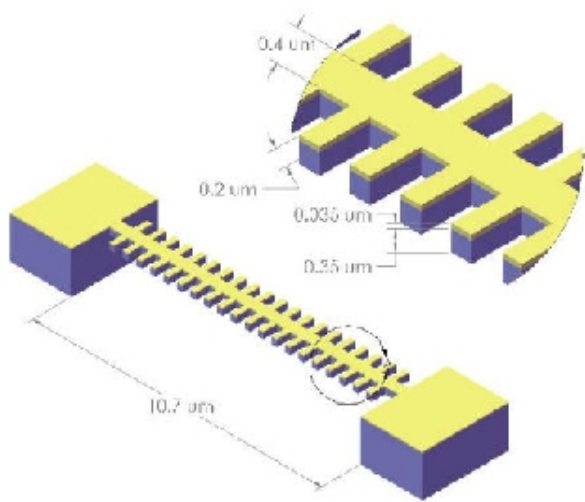


FIG. 1: Antenna structure.

dynamics of the system in which two resonant modes are coupled. This type of mode coupling, as we describe in detail, can allow detection of response in one mode by monitoring the coupled mode.

II. DISCRETE MODEL

A. Equations of motion

The antenna-like structure we investigate consists of a central clamped-clamped diamond beam with dimensions $L \times W \times h = 10.7\mu\text{m} \times 0.4\mu\text{m} \times 0.35\mu\text{m}$ and 40 perpendicular cantilevers with dimensions $l \times w \times h = 0.5\mu\text{m} \times 0.2\mu\text{m} \times 0.35\mu\text{m}$. The cantilevers are regularly spaced along the beam and symmetric with respect to the beam (see Fig. 1). There are $N = 20$ cantilevers on each side. In addition, the antenna is coated by a layer of gold whose length and width are those of the beam and whose thickness is $t = 0.035\mu\text{m}$. We denote by x the coordinate along the beam and by ξ the transverse one. The deflection of the beam with respect to its clamps is called $y(x, t)$ and the deflection of the j th lateral cantilever with respect to $y(x_j, t)$ is denoted by $\eta_j(\xi, t)$. In the following we shall only consider vibrational modes symmetric with respect to the central beam. The deflection of the cantilevers on either side of the beam are the same. They are described by the quantity $\eta_j(\xi, t)$. Considering that all the elements of the structure are one-dimensional and using the Euler-Bernoulli beam theory (see for example Ref. [25, 26, 27]), the equations of motion of the structure have the form

$$\mathcal{E}_b \frac{\partial^4 y}{\partial x^4} + \mu_b \frac{\partial^2 y}{\partial t^2} = -2\mathcal{E}_t \sum_{j=1}^N \left. \frac{\partial^3 \eta_j}{\partial \xi^3} \right|_{\xi=0} \delta(x - x_j) \quad (1)$$

$$\mathcal{E}_t \frac{\partial^4 \eta_j}{\partial \xi^4} + \mu_t \frac{\partial^2 \eta_j}{\partial t^2} = -\mu_t \frac{\partial^2 y_j}{\partial t^2}, \quad j \in \{1, \dots, N\} \quad (2)$$

where $y_j \equiv y(x_j, t)$ and together with the boundary conditions

$$y(0, t) = \frac{\partial y}{\partial x}(0, t) = y(L, t) = \frac{\partial y}{\partial x}(L, t) = 0 \quad (3)$$

$$\eta_j(0, t) = \frac{\partial \eta_j}{\partial \xi}(0, t) = \frac{\partial^2 \eta_j}{\partial \xi^2}(l, t) = \frac{\partial^3 \eta_j}{\partial \xi^3}(l, t) = 0, \quad (4)$$

with $j \in \{1, \dots, N\}$. The rigidities of the beam, \mathcal{E}_b , and the cantilevers, \mathcal{E}_t - that account for the presence of the gold layer - are respectively given by (see e.g. Ref. [26])

$$\mathcal{E}_b = \frac{W}{12} \frac{[E_d^2 h^4 + E_d E_g (4h^3 t + 6h^2 t^2 + 4ht^3) + E_g^2 t^4]}{(E_d h + E_g t)}$$

$$\mathcal{E}_t = \frac{w}{W} \mathcal{E}_b. \quad (5)$$

where $E_d = 700$ GPa and $E_g = 45.6$ GPa are the measured Young's moduli of diamond and gold, respectively. The masses per unit length of the beam and a cantilever are respectively given by

$$\mu_b = W(\rho_d h + \rho_g t) ; \quad \mu_t = \frac{w}{W} \mu_b \quad (6)$$

where $\rho_d = 4050$ kg.m⁻³ and $\rho_g = 19500$ kg.m⁻³ are the densities of diamond and gold, respectively. It is important to note that because of the smallness of E_g with respect to E_d , the rigidities of the beam and the cantilever are barely affected by the presence of the gold layer (roughly 2.5 % higher). This is in contrast with their linear mass that the gold layer increases by roughly 50 %. Thus, the presence of the gold layer merely increases the mass of the antenna without affecting its rigidity.

The force density in the r.h.s of equation (1) represents the shear force densities exerted by the cantilevers on the beam. No momenta appear in this equation because, for modes that are symmetric with respect to the central beam, the momenta exerted by two opposite cantilevers cancel each other. The r.h.s. of equation (2) is due to the motion of the base of the cantilever that follows the motion of the central beam at $\xi = 0$.

B. Energy and Lagrangian

The system of equations (1) and (2) (for $j \in \{1, \dots, N\}$) conserves the energy

$$H_d = \int_0^L dx \left[\frac{\mathcal{E}_b}{2} \left(\frac{\partial^2 y}{\partial x^2} \right)^2 + \frac{\mu_b}{2} \left(\frac{\partial y}{\partial t} \right)^2 \right] + 2 \sum_{j=1}^N \int_0^l d\xi \left[\frac{\mathcal{E}_t}{2} \left(\frac{\partial^2 \eta_j}{\partial \xi^2} \right)^2 + \frac{\mu_t}{2} \left(\frac{\partial \eta_j}{\partial t} + \frac{\partial y_j}{\partial t} \right)^2 \right]. \quad (7)$$

The first and second terms in Eq. (7) represent the elastic and kinetic energies of the central beam and of the $2N$

cantilever, respectively. Similar to Hamiltonian (7), the Lagrangian of the antenna, \mathcal{L}_d , is expressed as

$$\mathcal{L}_d = \int_0^L dx \left[\frac{\mu_b}{2} \left(\frac{\partial y}{\partial t} \right)^2 - \frac{\mathcal{E}_b}{2} \left(\frac{\partial^2 y}{\partial x^2} \right)^2 \right] + 2 \sum_{j=1}^N \int_0^l d\xi \left[\frac{\mu_t}{2} \left(\frac{\partial \eta_j}{\partial t} + \frac{\partial y_j}{\partial t} \right)^2 - \frac{\mathcal{E}_t}{2} \left(\frac{\partial^2 \eta_j}{\partial \xi^2} \right)^2 \right]. \quad (8)$$

Eqs. (1)-(2) can be established from the least action principle $\delta \mathcal{S}_d = 0$, i.e. $\frac{\delta \mathcal{S}_d}{\delta y} = 0$ and $\frac{\delta \mathcal{S}_d}{\delta \eta_j} = 0$, where the action is given by $\mathcal{S}_d = \int \mathcal{L}_d dt$.

C. Vibrational modes

The vibrational modes of Eqs. (1)-(4) can be found as follows. Given the punctual nature of the force densities, Eq. (1) reduces to

$$\mathcal{E}_b \frac{\partial^4 y}{\partial x^4} + \mu_b \frac{\partial^2 y}{\partial t^2} = 0 \quad \text{for } x \in [0, L], x \neq x_j, \quad (9)$$

with $j \in \{1, \dots, N\}$. At all points x_j , the function $y(x, t)$ and its first and second derivatives are continuous. But its third derivative is discontinuous and its discontinuity is obtained by integrating Eq. (1) over an infinitesimally small interval centered around x_j . Thus, in addition to the boundary conditions given in Eq. (3), $4N$ other conditions apply: the continuity of $y(x, t)$ and its first and second derivatives at $x = x_j$, $j \in \{1, \dots, N\}$, and

$$\mathcal{E}_b \left(\frac{\partial^3 y}{\partial x^3}(x_j^+, t) - \frac{\partial^3 y}{\partial x^3}(x_j^-, t) \right) = -2\mathcal{E}_t \frac{\partial^3 \eta_j}{\partial \xi^3}(0, t). \quad (10)$$

To simplify the system of Eqs. (1)-(2), as well as the boundary conditions, we shall work with the following non-dimensional quantities

$$u = \frac{x}{L}; \quad v = \frac{\xi}{l}; \quad \mu^4 = \frac{\mu_b L^4 \omega^2}{\mathcal{E}_b}; \quad \gamma^4 = \frac{\mu_t l^4 \omega^2}{\mathcal{E}_t}; \quad R = 2 \left(\frac{L}{l} \right)^3 \frac{\mathcal{E}_t}{\mathcal{E}_b}. \quad (11)$$

Looking for mode solutions on the form $y(x, t) = Y(u) \cos(\omega t)$ and $\eta_j(\xi, t) = H_j(v) \cos(\omega t)$, the equations to be solved become

$$\frac{d^4 Y(u)}{du^4} - \mu^4 Y(u) = 0 \quad \text{for } u \in [0, 1], u \neq u_j, \quad (12)$$

$$\frac{d^4 H_j(v)}{dv^4} - \gamma^4 (H_j(v) + Y(u_j)) = 0, \quad (13)$$

and the boundary conditions (3), (4) and (10) read

$$\begin{aligned} Y(0) &= Y'(0) = Y(1) = Y'(1) = 0, \\ Y(u_j^-) &= Y(u_j^+); \quad Y'(u_j^-) = Y'(u_j^+); \\ Y''(u_j^-) &= Y''(u_j^+); \quad Y'''(u_j^+) - Y'''(u_j^-) = -RH_j'''(0), \\ H_j(0) &= H_j'(0) = H_j''(1) = H_j'''(1) = 0, \end{aligned} \quad (14)$$

where $u_j = j/(N+1)$, $j \in \{1, \dots, N\}$. The solution to the system of equations (12)-(13) is worked out in appendix A. From it, we eventually obtain the secular equation of the discrete model

$$\det \mathbf{M}(\omega) = 0, \quad (15)$$

where $\mathbf{M}(\omega)$ is a 2×2 matrix given by

$$\mathbf{M}(\omega) = \mathbf{T}(\mu) \left[\prod_{j=1}^N (\mathbb{1} + 2\alpha A_2(\gamma) \mathbf{K}_j(\mu)) \right] \mathbf{L}. \quad (16)$$

In the expression above, $\mathbb{1}$ is the 4×4 unity matrix, $\alpha = w/W$, $A_2(\gamma)$ is defined in Eq. (30). The quantities μ and γ , defined in (11), are related to each other as $\mu = \gamma L/l$. They are the frequency dependent parameters of Eq. (16). Finally, the matrices $\mathbf{K}_j(\mu)$, $\mathbf{T}(\mu)$ and \mathbf{L} are given by

$$\mathbf{K}_j(\mu) = \begin{pmatrix} s_j c_j & s_j^2 & s_j \cdot ch_j & s_j \cdot sh_j \\ -c_j^2 & -c_j s_j & -c_j \cdot ch_j & -c_j \cdot sh_j \\ -c_j \cdot sh_j & -s_j \cdot sh_j & -sh_j \cdot ch_j & -sh_j^2 \\ c_j \cdot ch_j & s_j \cdot ch_j & ch_j^2 & ch_j \cdot sh_j \end{pmatrix}$$

$$\mathbf{L} = \begin{pmatrix} 1 & 0 \\ 0 & 1 \\ -1 & 0 \\ 0 & -1 \end{pmatrix}; \quad \mathbf{T}(\mu) = \begin{pmatrix} \cos \mu & -\sin \mu \\ \sin \mu & \cos \mu \\ \cosh \mu & \sinh \mu \\ \sinh \mu & \cosh \mu \end{pmatrix}^T. \quad (17)$$

where \mathbf{A}^T denotes the transpose of \mathbf{A} and where $c_j \equiv \cos(\mu u_j)$; $s_j \equiv \sin(\mu u_j)$; $ch_j \equiv \cosh(\mu u_j)$; $sh_j \equiv \sinh(\mu u_j)$; $u_j = j/(N+1)$. Using this, we obtain the exact solution of the discrete model. Nonetheless, the method is particularly tedious in practice and it does not allow for an easy analytical investigation of the problem unless the number of cantilevers to be treated is very small. The case $N = 1$ is treated in appendix B and compared to the result given by the continuum approach developed hereafter.

III. CONTINUUM APPROXIMATION

A. Derivation of the model

We now derive a continuum approximation for the system of Eqs. (1)-(4). The idea is to ‘‘smooth out’’ the punctual force densities of Eq. (1) in such a way that the total shear force exerted by the j th cantilever on the beam is the same but with a density that is continuous along the beam. The shear force exerted by the two cantilevers in the j th position is given by $F_j = -2\mathcal{E}_t (\partial^3 \eta_j / \partial \xi^3)(0, t)$. Averaging its effect over the interval $[x_j - \delta/2, x_j + \delta/2]$ produces the force density $f_j = F_j / \delta$ and filling the gap between the cantilevers requires $\delta = L/N$. Using this, we obtain a piecewise-constant force density given by $f_j = -(2N\mathcal{E}_t/L) (\partial^3 \eta_j / \partial \xi^3)(0, t)$ whose continuous version is

straightforward if we now assume that the cantilevers form a continuum along the beam. Writing $\eta_j(\xi, t) \equiv \eta(x_j, \xi, t)$, the continuous version of the density simply reads $f(x) = -(2N\mathcal{E}_t/L)(\partial^3\eta/\partial\xi^3)(x, 0, t)$. Therefore, the equations of motion become

$$\mathcal{E}_b \frac{\partial^4 y(x, t)}{\partial x^4} + \mu_b \frac{\partial^2 y(x, t)}{\partial t^2} = -\frac{2\mathcal{E}_t N}{L} \frac{\partial^3 \eta(x, \xi, t)}{\partial \xi^3} \Big|_{\xi=0} \quad (18)$$

$$\mathcal{E}_t \frac{\partial^4 \eta(x, \xi, t)}{\partial \xi^4} + \mu_t \frac{\partial^2 \eta(x, \xi, t)}{\partial t^2} = -\mu_t \frac{\partial^2 y(x, t)}{\partial t^2}, \quad (19)$$

with clamped-clamped and cantilever-like boundary conditions for the central beam and the cantilevers, respectively

$$y(0, t) = \frac{\partial y}{\partial x}(0, t) = y(L, t) = \frac{\partial y}{\partial x}(L, t) = 0 \quad (20)$$

$$\eta(x, 0, t) = \frac{\partial \eta}{\partial \xi}(x, 0, t) = \frac{\partial^2 \eta}{\partial \xi^2}(x, l, t) = \frac{\partial^3 \eta}{\partial \xi^3}(x, l, t) = 0. \quad (21)$$

This model is of course expected to provide better results as the density of cantilevers increases. Equations (18)-(19) conserve the following energy

$$H_c = \int_0^L dx \left[\frac{\mathcal{E}_b}{2} \left(\frac{\partial^2 y}{\partial x^2} \right)^2 + \frac{\mu_b}{2} \left(\frac{\partial y}{\partial t} \right)^2 \right] + \frac{2N}{L} \int_0^L dx \int_0^l d\xi \left[\frac{\mathcal{E}_t}{2} \left(\frac{\partial^2 \eta}{\partial \xi^2} \right)^2 + \frac{\mu_t}{2} \left(\frac{\partial \eta}{\partial t} + \frac{\partial y}{\partial t} \right)^2 \right]. \quad (22)$$

Similar to the equations of the discrete model (1)-(2), Eqs. (18)-(19) can be deduced from the least action principle $\delta\mathcal{S}_c = 0$, where $\mathcal{S}_c = \int \mathcal{L}_c dt$ and where the Lagrangian \mathcal{L}_c is obtained from Hamiltonian (22) by changing the sign of the elastic energy terms.

The continuum model presented above becomes more accurate as the density of cantilevers, N/L , increases. To get a sense of its limitations though, let us imagine that, for a given mode, the shape of the central beam has $n-1$ nodes, and consequently n ‘‘arches’’. We then expect that the model holds if at least one cantilever per arch subsists, which basically yields the following condition of validity of the continuum model,

$$n < N. \quad (23)$$

Indeed, should condition (23) fail to be satisfied, the ‘‘cantilever continuum’’ would create some inertial effects on an arch where no physical cantilever is to be found, which is not desirable. The limit of a single cantilever per arch, instead of two or more, can still appear rather arbitrary. But a comparison of the lower part of the spectrum of the continuum and discrete models for $N = 1$ done in appendix B reveals that their first frequencies are very similar. Therefore, thinking of the central beam as a collection of sub-beams (arches) pinned at the level of its nodes, it seems reasonable to take one cantilever per arch as the limit of validity of the continuum model.

B. Vibrational modes

Working again with the non-dimensional quantities defined in Eq. (11), we look for mode solutions of the form

$$y(x, t) = Y(u) \cos(\omega t) \quad ; \quad \eta(x, \xi, t) = H(u, v) \cos(\omega t). \quad (24)$$

The equations of motion (18) and (19) become

$$\frac{d^4 Y(u)}{du^4} - \mu^4 Y(u) = -RN \frac{\partial^3 H}{\partial v^3}(u, 0) \quad (25)$$

$$\frac{\partial^4 H(u, v)}{\partial v^4} - \gamma^4 (H(u, v) + Y(u)) = 0 \quad (26)$$

with boundary conditions

$$Y(0) = \frac{dY}{du}(0) = Y(1) = \frac{dY}{du}(1) = 0 \quad (27)$$

$$H(u, 0) = \frac{\partial H}{\partial v}(u, 0) = \frac{\partial^2 H}{\partial v^2}(u, 1) = \frac{\partial^3 H}{\partial v^3}(u, 1) = 0. \quad (28)$$

Now, solving Eq. (26) yields

$$\begin{aligned} H(u, v) &= [A_1(\gamma) \cos(\gamma v) + A_2(\gamma) \sin(\gamma v) + \\ &\quad A_3(\gamma) \cosh(\gamma v) + A_4(\gamma) \sinh(\gamma v) - 1] Y(u) \\ &\equiv \tilde{H}(v) Y(u), \end{aligned} \quad (29)$$

where the coefficients $A_i(\gamma)$, determined by the boundary conditions (28), are given by

$$\begin{aligned} A_1(\gamma) &= \frac{1 + \cos \gamma \cosh \gamma - \sin \gamma \sinh \gamma}{2(1 + \cos \gamma \cosh \gamma)}, \\ A_2(\gamma) &= \frac{\cos \gamma \sinh \gamma + \sin \gamma \cosh \gamma}{2(1 + \cos \gamma \cosh \gamma)}, \\ A_3(\gamma) &= \frac{1 + \cos \gamma \cosh \gamma + \sin \gamma \sinh \gamma}{2(1 + \cos \gamma \cosh \gamma)}, \\ A_4(\gamma) &= -\frac{\cos \gamma \sinh \gamma + \sin \gamma \cosh \gamma}{2(1 + \cos \gamma \cosh \gamma)}. \end{aligned} \quad (30)$$

From these results we can calculate the r.h.s. of Eq. (25), $-RN\partial^3 H/\partial v^3(u, 0) = 2RN\gamma^3 A_2(\gamma)Y(u)$, and we finally obtain

$$\frac{d^4 Y(u)}{du^4} - \beta^4 Y(u) = 0, \quad (31)$$

with

$$\beta^4 = \mu^4 + \gamma^3 RN \frac{\cos \gamma \sinh \gamma + \sin \gamma \cosh \gamma}{1 + \cos \gamma \cosh \gamma}. \quad (32)$$

Eqs. (31) and (32) show that our continuum model reduces to a simple clamped-clamped beam equation with a parameter β that depends in a non trivial way upon the mode frequency ω . Indeed, according to Eq. (11), the parameters μ^4 and γ^4 are quadratic functions of the frequency and the parameters R and N are simply constants. Now, because Eq. (31) along with boundary conditions (27) is merely a clamped-clamped beam equation,

it can be solved to obtain

$$Y(u) = A \left\{ \cos(\beta u) - \cosh(\beta u) - \left(\frac{\cos \beta - \cosh \beta}{\sin \beta - \sinh \beta} \right) (\sin(\beta u) - \sinh(\beta u)) \right\}, \quad (33)$$

with the secular equation

$$\cos(\beta) \cosh(\beta) = 1. \quad (34)$$

C. Frequency spectrum of the continuum model: Band structure

We see that the shape of the vibrational modes of the central beam is uniquely determined by the parameter β solution to Eq. (34). The solutions β_n can be evaluated numerically: $\beta_1 = 4.730040745$, $\beta_2 = 7.853204624$, $\beta_3 = 10.99560784$, and $\beta_n \simeq (n+1/2)\pi$ as n is large. To a given β_n corresponds a single modal shape for the central beam, $Y_n(u)$, but an infinite number of modal shapes $H_{n,k}(u, v)$ and frequencies $\omega_{n,k}$, $k \geq 1$, obtained by solving Eq. (32) for ω . To see that the number of solutions to Eq. (32) for $\beta = \beta_n$ is infinite, we first rewrite it in terms of the variable γ by using $\mu = \gamma L/l$ and denoting by $m_b = L\mu_b$ and $m_t = l\mu_t$ the masses of the beam and of one cantilever, respectively, we finally find

$$Q(\gamma, \beta_n) \equiv \left(\cos \gamma + \frac{1}{\cosh \gamma} \right) \left[1 - \left(\frac{l\beta_n}{L\gamma} \right)^4 \right] + \frac{2Nm_t \cos \gamma \tanh \gamma + \sin \gamma}{m_b \gamma} = 0 \quad (35)$$

valid for $\cos \gamma \cosh \gamma + 1 \neq 0$. It becomes now clear that when γ is large, Eq. (35) reduces to $\cos \gamma = 0$. This equation has an infinite number of solutions with asymptotic behavior $\gamma_{n,k} = (k-1/2)\pi$ as $k \rightarrow \infty$. Interestingly, these asymptotic solutions are independent of all the parameters entering Eq. (35), and in particular, of β_n *provided the latter is finite, i.e. $n \not\rightarrow \infty$* . Finally, the frequency corresponding to a given value $\gamma_{n,k}$ is given by Eq. (11) as

$$\omega_{n,k} = \sqrt{\frac{\mathcal{E}_t}{\mu_t} \left(\frac{\gamma_{n,k}}{l} \right)^2}. \quad (36)$$

To understand the structure of the spectrum, we have plotted in Fig. 2 the frequencies $\omega_{n,k}$ normalized to the fundamental, $\omega_{1,1}$, for $N = 20$ and the antenna dimensions indicated in II A. As we can see, the spectrum consists of “bands” separated by gaps. The band number is the label k that we have attributed to the solution of Eq. (35), $\gamma_{n,k}$. To elucidate the appearance of bands, we note that as n increases, the solution to Eq. (34) becomes large and is asymptotically given by $\beta_n \sim (n+1/2)\pi$. For a finite solution, $\gamma_{\infty,k}$, of Eq. (32) to exist as $n \rightarrow \infty$, the denominator of the second term of the r.h.s of (32) needs to vanish. Hence,

$$1 + \cos(\gamma_{\infty,k}) \cosh(\gamma_{\infty,k}) = 0. \quad (37)$$

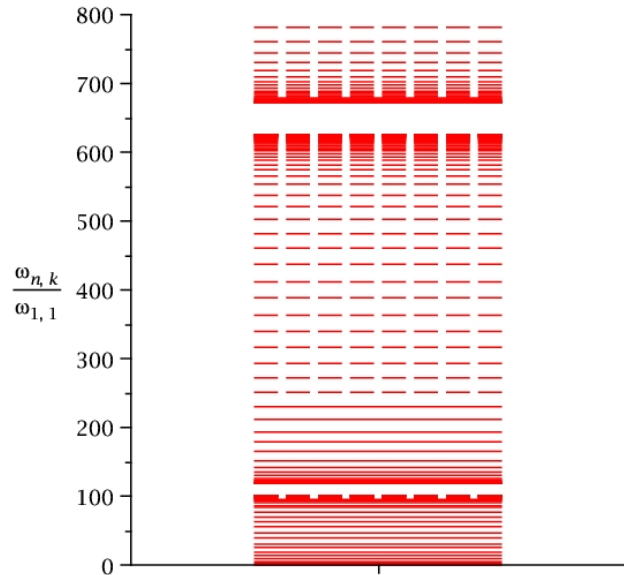


FIG. 2: Frequency spectrum obtained from Eq. (35) for $N = 20$ and the antenna parameters given in II A. Solid lines correspond to $n < N$ (physically relevant frequencies) and dashed ones to $n > N$.

This equation is the well-known secular equation for a simple cantilever. It provides here the upper band edge of the k th band whose frequency, determined by Eq. (36), reads

$$\omega_{\infty,k} = \sqrt{\frac{\mathcal{E}_t}{\mu_t} \left(\frac{\gamma_{\infty,k}}{l} \right)^2}. \quad (38)$$

For the case at hand, we have $\omega_{\infty,1}/\omega_{1,1} \simeq 100.103$, $\omega_{\infty,2}/\omega_{1,1} \simeq 627.336$ and $\omega_{\infty,k}/\omega_{1,1} \simeq ((k-1/2)\pi/\gamma_{1,1})^2$ with $\gamma_{1,1} \simeq 0.187413$ for $k \geq 3$. It is easy to see that the accuracy of the latter formula improves exponentially as k increases. For $k = 3$ the relative error to the exact result is already as small as 0.02%. An approximate analytical expression for $\gamma_{1,1}$ is given in the next section while results for the lower edge of the k th band, $\gamma_{1,k}$, $k \geq 2$, will be given in section III E.

At the edges of each band but the lower edge of the first one that we shall refer to as the “fundamental band”, frequencies clearly accumulate. However, close to the lower band edge, a finite number of frequencies cluster while an infinite number accumulate at the upper band edge. Each band contains all possible values of β_n , $1 \leq n \leq \infty$, i.e. all possible modal shapes for the central beam, $Y_n(u)$. Even though modes with the same shape $Y_n(u)$ repeatedly appear within each band, they differ from band to band because their cantilever continuum, $H_{n,k}(u, v)$, depends on $\gamma_{n,k}$ that is, on both n and k (see Eq. (29)). Note also that, within a given band, the frequency increases with the excitation level of the central beam.

At mid-band, modal frequencies are somewhat sparse and more regularly spaced than at the boundaries. This

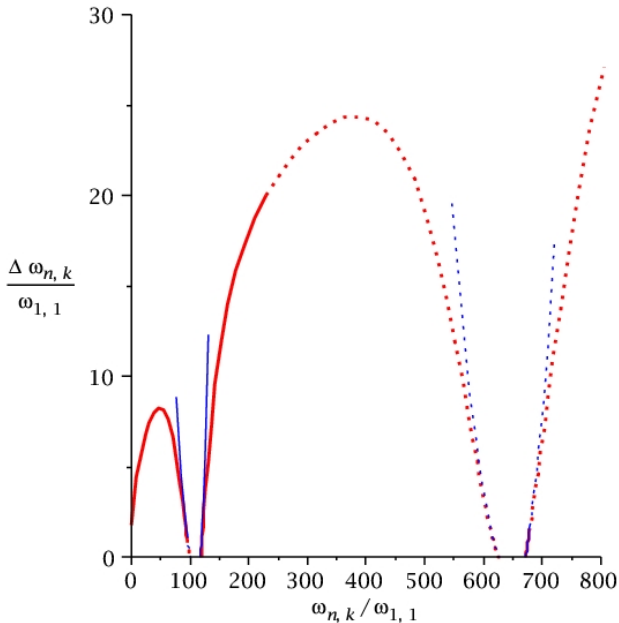


FIG. 3: Frequency spacing, $(\omega_{n+1,k} - \omega_{n,k})/\omega_{1,1}$, versus frequency (in red) for the same parameters as in Fig. 2. In blue, analytical results obtained from Eq. (39). Curves are solid for $n < N$ and dotted for $n > N$.

is confirmed in Fig. 3 that displays the normalized spacing between two consecutive frequencies versus the normalized frequency itself. Notice that, the inverse of this function is nothing but the normalized “density of states” of the spectrum. Mid-band frequencies can be approximately evaluated once we note that the function $A_2(\gamma)$ appearing in secular equation (32) is small away from the boundaries $\gamma_{\infty,k}$ given by Eq. (37) and increases slowly and regularly in this region. Rewriting Eq. (32) as $\mu^4 - \beta_n^4 + 4\alpha N A_2(\mu l/L)\mu^3 = 0$, we seek a solution close to $\mu \sim \beta_n$. With a first Newton iteration we obtain

$$\gamma_{n,k} \simeq \gamma_n^{(0)} \left[1 - \frac{\alpha N A_2(\gamma_n^{(0)})}{\beta_n + 3\alpha N A_2(\gamma_n^{(0)}) + \alpha N \beta_n \frac{l}{L} A_2'(\gamma_n^{(0)})} \right],$$

$$|\beta_n - \mu_k^*| \ll \frac{L \Delta_k}{2l}. \quad (39)$$

where $\gamma_n^{(0)} = \frac{\beta_n l}{L}$, $\alpha = w/W$ and $A_2(\gamma)$ is given in Eq. (30). In the last equation, $\Delta_k = \gamma_{\infty,k} - \gamma_{1,k}$, is the width of band k and μ_k^* is determined as the solution to $A_2(\mu_k^* l/L) = 0$. For k large enough, $\mu_k^* \simeq (k - 1/4)\pi l/L$, $k \geq 1$. In this case, we have also $\beta_n \simeq (n + 1/2)\pi$, $n \geq 1$. Approximating the bandwidth by $\Delta_k \simeq \gamma_{\infty,k} - \gamma_{\infty,k-1} \simeq \pi$ as k is large enough, the condition of Eq. (39) becomes $|(n + 1/2)l/L - (k - 1/4)| \ll 1/2$, which provides bounds on the beam excitation (n) of band k for which (39) is valid. In this case Eq. (39) simplifies to

$$\gamma_{n,k} \simeq \frac{l}{L} \left[\beta_n - \alpha N A_2 \left(\frac{\beta_n l}{L} \right) \right], \quad |\beta_n - \mu_k^*| \ll \frac{L \Delta_k}{2l}. \quad (40)$$

Although simple, this last expression is not very accurate for the first bands.

Very few of the many frequencies occurring in the spectrum of the continuum model can be detected experimentally. This is mainly due to the modal response of the structure which, for a given driving power, is drastically suppressed as its excitation level increases as we shall prove in the study of a damped driven antenna done in section III H. Moreover, the antenna is generally driven by a harmonic force that is constant over the beam which does not allow for the observation of antisymmetric modes, $Y_n(u)$ with n even. In what follows, we show how to evaluate the frequency of the fundamental mode of the structure and explain the clustering phenomenon observed at both edges of each band.

D. Small γ solution, fundamental mode and mass loading

If a small solution to Eq. (35) exists, $\gamma \ll 1$, we can obtain its approximate expression by expanding Eq. (35) around $\gamma = 0$. In this case we find that

$$\gamma \simeq \left(\frac{\mu_b}{\mu_a} \right)^{1/4} \frac{l\beta}{L}, \quad (41)$$

where $\mu_a = (m_b + 2Nm_t)/L$ is the mass per unit length of the entire antenna (beam plus cantilevers). Replacing this result in Eq. (36) and using the fact that $(\mu_t \mathcal{E}_b)/(\mu_b \mathcal{E}_t) = 1$ (see Eqs. (5) and (6)) yields

$$\omega \simeq \sqrt{\frac{\mathcal{E}_b}{\mu_a}} \left(\frac{\beta}{L} \right)^2. \quad (42)$$

In this limit, the inertia of the cantilevers is negligible and the frequency of the vibrational mode is the frequency of a clamped-clamped beam whose mass per unit length includes the mass of the central beam plus the mass of the cantilevers. According to Eqs. (29) and (30), the mode shape $H(u, v)$ corresponding to this small γ solution is found to be

$$H(u, v) \simeq \frac{\gamma^4}{24} v^2 (v^2 - 4v + 6) Y(u). \quad (43)$$

Notice that this function is proportional to γ^4 and is very small. This confirms that the cantilevers hardly move at all and that their mass only loads the central beam. Finally, given our parameters, the condition $\gamma \ll 1$ is typically satisfied for the first positive root of Eq. (35) when $\beta = \beta_1$. It is then valid for $\gamma_{1,1}$, i.e. for the fundamental mode. Indeed, using Eq. (41) and the antenna parameters of section II A, we find $\gamma_{1,1} \simeq 0.1874150\dots$ while the exact numerical value reads $\gamma_{1,1} = 0.1874136\dots$, i.e. a relative error of $7 \times 10^{-4} \%$.

E. Frequency clustering

The *frequency clustering* evoked in III C, which has also been observed numerically in 3D finite-element simula-

tions, can be explained with the help of secular equation (32). To evaluate the accumulation of frequencies occurring at the upper edge of the k th band ($\omega_{\infty,k}$) and at the lower edge of the $(k+1)$ th band, we seek a perturbative solution of Eq. (32) around $\gamma \sim \gamma_{\infty,k}$ given in Eq. (37). Using Eq. (35) and $\gamma_{n,\tilde{k}} \simeq \gamma_{\infty,k} - Q(\gamma_{\infty,k}, \beta_n)/Q'(\gamma_{\infty,k}, \beta_n)$, where \tilde{k} stands either for k or $k+1$, and Q' is the derivative of Q with respect to γ , we obtain

$$\gamma_{n,\tilde{k}} \simeq \gamma_{\infty,k} + \left\{ \frac{L\gamma_{\infty,k}}{2\alpha Nl} \left(\frac{t_{\gamma_{\infty,k}} - th_{\gamma_{\infty,k}}}{t_{\gamma_{\infty,k}} + th_{\gamma_{\infty,k}}} \right) \left[1 - \left(\frac{l\beta_n}{L\gamma_{\infty,k}} \right)^4 \right] + th_{\gamma_{\infty,k}} - \frac{2}{t_{\gamma_{\infty,k}} + th_{\gamma_{\infty,k}}} + \frac{1}{\gamma_{\infty,k}} \right\}^{-1}, \quad (44)$$

where $t_\gamma = \tan \gamma$ and $th_\gamma = \tanh \gamma$. This solution is valid as far as the corrective term is very small compared to $\gamma_{\infty,k}$. This leads to the two conditions below.

1. Upper band edge

With respect to the frequency clustering at the upper band edge of the k th band, Eq. (44) starts to be valid as soon as β_n is large enough. In this case, it is easy to see that this approximately leads to the condition

$$\beta_n \gg \frac{L\gamma_{\infty,k}}{l} \left(1 + \frac{2\alpha Nl}{L} \right)^{1/4}. \quad (45)$$

This condition can always be satisfied for large enough n , given that in this case, $\beta_n \simeq (n+1/2)\pi$ (for simplicity, we have discarded the term $(t_{\gamma_{\infty,k}} - th_{\gamma_{\infty,k}})/(t_{\gamma_{\infty,k}} + th_{\gamma_{\infty,k}})$ that is close to unity). The longer the cantilever, the easier the condition (45) to be satisfied. For an antenna structure with high cantilever to beam length ratio, we may expect to observe a clustering of modes around the frequency determined in (38). Experimentally, however, this very much depends on the sensitivity of the measuring device given that highly excited modes for the beam are difficult to detect. Moreover, the range of validity of our model, determined by the condition $n < N$, restricts the possibility of observing the beginning of an upper edge clustering to the fundamental band.

Provided (45) is satisfied, Eq. (44) simplifies to

$$\begin{aligned} \gamma_{n,k} - \gamma_{\infty,k} &\simeq \frac{NR\gamma_{\infty,k}^3}{\beta_n^4} \left(\frac{th_{\gamma_{\infty,k}} + t_{\gamma_{\infty,k}}}{th_{\gamma_{\infty,k}} - t_{\gamma_{\infty,k}}} \right) \\ &= -\frac{NR\gamma_{\infty,k}^3}{\beta_n^4} \left(\frac{th_{\gamma_{\infty,k}} + t_{\gamma_{\infty,k}}}{th_{\gamma_{\infty,k}} t_{\gamma_{\infty,k}}} \right)^2. \end{aligned} \quad (46)$$

The second equality has been obtained from (37). As we can see, the corrective term to $\gamma_{\infty,k}$ is always negative which confirms that the frequencies are indeed accumulating at the upper edge of the band as n increases. It is also possible to show that the (adequately normalized) modal shape of the cantilever corresponding to $\omega_{n,k}$ factorizes asymptotically as the product of the k th mode of a

simple cantilever by the n th mode of a clamped-clamped beam, $H_{n,k}(u, v) \sim \phi_k(v)Y_n(u)$ as $n \rightarrow \infty$. Thus, as the excitation of the beam becomes high enough, the modal shape of the antenna is given by a simple cantilever mode modulated by the profile of the central beam. The same result is obtained for a weakly dissipative driven antenna in III H 3.

2. Lower band edge

A frequency clustering at the lower edge of each band does not always occur. This essentially depends on the geometry of the antenna. For the correction given in Eq. (44) to be valid,

$$\beta_n \ll \frac{L\gamma_{\infty,k}}{l} \left[1 - \frac{2\alpha Nl}{L} \left(\frac{th_{\gamma_{\infty,k}} + t_{\gamma_{\infty,k}}}{th_{\gamma_{\infty,k}} - t_{\gamma_{\infty,k}}} \right) \right]^{1/4} \quad (47)$$

has to be satisfied. For large cantilever to beam length ratio, however, inequality (47) cannot be satisfied because the square-bracketed term becomes negative. This means either that expanding the secular equation around the upper edge of the k th band does not provide any reliable information on the lower edge of the $(k+1)$ th band or simply that no clustering occurs at the lower band edge. For the geometry of the antenna described in the introduction, frequency clustering occurs and the band gap $\Delta_{k,k+1}$ between the k th and $(k+1)$ th bands can be accurately evaluated with the help of Eq. (44) as

$$\Delta_{k,k+1} \equiv \gamma_{1,k+1} - \gamma_{\infty,k}. \quad (48)$$

This expression is accurate to less than 5% for the first gap and to less than 0.5% for the second one and its accuracy improves drastically as k increases.

F. Energy and Lagrangian

1. Modal energy

Using expressions (22) and (24-34), we can evaluate the energy $E_{n,k}$ of the mode $\varphi_{n,k} = (y_n(x, t), \eta_{n,k}(x, \xi, t))^T$. After some algebra, we find

$$E_{n,k} = \frac{M_{n,k} A^2 \omega_{n,k}^2}{2}, \quad (49)$$

where

$$M_{n,k} = m_b + 2Nm_t L_{n,k}. \quad (50)$$

The quantity $L_{n,k}$, that takes into account the dynamics of the cantilevers at the level of the effective mass $M_{n,k}$, is given by $L_{n,k} = L(\gamma_{n,k})$ where, defining $h(v) \equiv \tilde{H}(v) + 1$,

$$L(\gamma) = \int_0^1 h^2(v) dv = \frac{1}{4} \left(\frac{\cos \gamma + \cosh \gamma}{1 + \cos \gamma \cosh \gamma} \right)^2 + \frac{3}{2} \frac{A_2(\gamma)}{\gamma}. \quad (51)$$

Incidentally, we also note a relation that will prove useful when dealing with the motion of a driven weakly damped structure in section III H 5

$$L(\gamma) = \frac{1}{2\gamma^3} \frac{d}{d\gamma} (\gamma^3 A_2(\gamma)). \quad (52)$$

Eq. (49) is exactly the energy of an effective harmonic oscillator with amplitude A , frequency $\omega_{n,k}$ and mass $M_{n,k}$. Notice that, according to our definition of $Y(u)$ in (33), the amplitude is defined as $A^2 = \int_0^1 Y_n^2(u) du$ which is independent of n and k . Other definitions of the amplitude (like the maximal deflection of the central beam at the mid point, for example) are typically mode-dependent and redefine the effective mass of the structure. As we see, the effective mass of the antenna is renormalized by the factor $L_{n,k}$ that affects the total mass of the cantilevers, $2Nm_t$. In the specific case of the fundamental mode, we have shown in the previous section that $\gamma_{1,1} \ll 1$. Therefore, $L_{1,1} \simeq 1$ and the effective mass of the antenna, $M_{1,1} \simeq m_b + 2Nm_t$, is its actual mass. This confirms the finding of section III D that in the fundamental mode the cantilevers have a pure mass loading effect. We can also use Eq. (49) to define an effective mode-dependent spring constant $\kappa_{n,k}$ as

$$\kappa_{n,k} = M_{n,k} \omega_{n,k}^2. \quad (53)$$

Once again, this result depends on the definition chosen for the amplitude and is valid here for $A^2 = \int_0^1 Y_n^2(u) du$.

2. Energy partition

To complete the modal analysis of the antenna, we evaluate the energy partition of each mode that is, we compare the energies of the cantilever continuum and of the central beam to understand which part of the structure is the most active. For a mode, the elastic energies of the central beam and the cantilever continuum reach their maximum at the same time and at this point their kinetic energy is zero. The sum of the maximal elastic energies of the beam and the continuum is then equal to the total energy of the system. We thus choose to calculate the ratio, $r_{n,k}$, of the maximal elastic energy of the beam, $U_{b;n,k}$, to the total energy of the structure, $E_{n,k}$, as a function of the frequency of the mode, $\omega_{n,k}$. The function $r_{n,k}$ ranges from 0 to 1 and is expected to be useful in the design of antenna structures with a specific task. The central beam elastic energy is given by

$$U_b[y(x,t)] = \int_0^L dx \left[\frac{\mathcal{E}_b}{2} \left(\frac{\partial^2 y}{\partial x^2} \right)^2 \right]. \quad (54)$$

Using expressions (24-34), we obtain

$$\begin{aligned} U_{b;n,k} &\equiv \max_t U_b[Y_n(x/L) \cos(\omega_{n,k}t)] = \frac{\mathcal{E}_b}{2L^3} A^2 \beta_n^4 \\ &= Nm_t A^2 \omega_{n,k}^2 \left(\frac{m_b}{2Nm_t} + 2 \frac{A_2(\gamma_{n,k})}{\gamma_{n,k}} \right). \end{aligned} \quad (55)$$

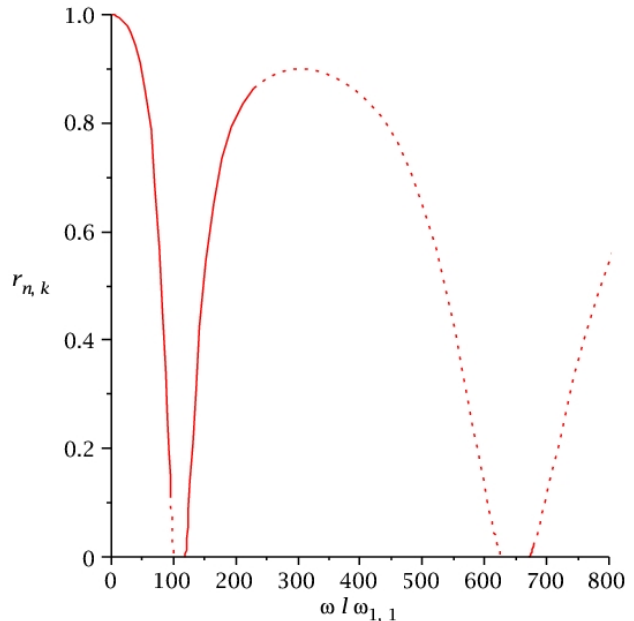


FIG. 4: Ratio, $r_{n,k}$ (see Eq. (56)), of the maximal elastic energy of the beam to the total energy of the antenna versus the normalized frequency, $\omega_{n,k}/\omega_{1,1}$. Antenna parameters are given in section II A and $N = 20$. Solid lines indicate physically relevant results for the continuum model ($n < N$) and dotted lines the results for ($n > N$).

Using expression (49) for the total energy $E_{n,k}$, we finally have

$$r_{n,k} \equiv \frac{U_{b;n,k}}{E_{n,k}} = \left(\frac{\frac{m_b}{2Nm_t} + 2 \frac{A_2(\gamma_{n,k})}{\gamma_{n,k}}}{\frac{m_b}{2Nm_t} + L_{n,k}} \right), \quad (56)$$

where $L_{n,k}$ is given in Eq. (51). In Fig. 4 we display $r_{n,k}$ versus the normalized frequency $\omega_{n,k}/\omega_{1,1}$. We observe that at the edges of all the bands but the lower edge of the first one, $r_{n,k}$ almost vanishes. This means that most of the energy of the structure is located in the cantilever continuum. By contrast, in the middle of the bands, most of the energy is stored in the central beam. This confirms the results of the previous sections showing that close to the band edges, the parameter γ almost satisfies the “cantilever” secular equation $1 + \cos \gamma \cosh \gamma = 0$, which clearly indicates that the spectrum is mainly governed by the dynamics of the cantilever continuum in this region while in the “middle” of the bands, $\gamma_{n,k} \sim (l/L)\beta_n$ (see Eq. (40)), which makes the spectrum close to that of a clamped-clamped beam. The peculiarity of the first band lies in the fact that for $\gamma_{n,1}$ close enough to zero, $r_{n,1} \sim 1 - \gamma_{n,1}^4/[20(\sigma + 1)]$ where $\sigma = m_b/2Nm_t$. The energy of the very first modes and, in particular, the fundamental, is thus essentially stored in the beam. This confirms the results obtained in section III D.

3. Lagrangian

It is also interesting to evaluate the Lagrangian $\mathcal{L}_{n,k}(t)$ of the system and in particular its time average that we will use in the next section to evaluate the effects of small nonlinearities and damping on the structure. We find

$$\mathcal{L}_{n,k}(t) = -\frac{M_{n,k}A^2\omega_{n,k}^2}{2}\cos(2\omega_{n,k}t) \Rightarrow \langle \mathcal{L}_{n,k}(t) \rangle = 0, \quad (57)$$

where $\langle \dots \rangle$ denotes the time average. The modal Lagrangian of the linear continuum model is then similar to a harmonic oscillator's and its time average is zero. This result will be used in the perturbative treatment of a weakly nonlinear and dissipative antenna in section IV.

G. Fundamental and first collective modes: comparison with finite-element results

In this section, we compare the results of our continuum model (CM) to those obtained with a finite element method (FE) that treats the vibrations of the antenna within the frame of three-dimensional elasticity theory. We are primarily interested in the fundamental and first collective modes, that is in the first modes of the first and second band, respectively. These modes are easy to observe experimentally. They are related to the parameters $\gamma_{1,1}$ and $\gamma_{1,2}$, respectively. Using Eq. (35) and the antenna parameters given in II A, we find that the two first roots of $Q(\gamma, \beta_1)$ with $\beta_1 = 4.73004\dots$ are $\gamma_{1,1} = 0.187413\dots$ and $\gamma_{1,2} = 2.046440\dots$. If we use Eq. (41), one finds $\gamma_{1,1} \simeq 0.187415$. It shows that this approximate solution is very reliable for the fundamental frequency. The corresponding frequency, obtained from Eq. (36), is $f_{1,1} = \omega_{1,1}/2\pi \simeq 24.7$ MHz, slightly higher than the frequency observed in simulations (23.6 MHz). This might be explained by the effective cross-sectional stiffness that we approximate for the two material layers. The frequency of the first collective mode calculated from $\gamma_{1,2} = 2.046440$ is $f_{1,2} \simeq 2.94$ GHz which is much higher than $f_{1,2}^{\text{FE}} \simeq 1.51$ GHz, the frequency from finite element simulations. A reason for this discrepancy is that all elements of the antenna structure are considered as one-dimensional in our model. Consequently, their length is the only dimension taken into account in the dynamics of the system. However, in the real structure, the central beam has a nonzero width, W , on the order of the cantilever length, l . For motions of the cantilevers comparable to the beam's, the shear momentum they exert on both of its sides becomes large enough to bend it *laterally* with respect to its mid-line, an occurrence indeed confirmed by our three-dimensional finite-element simulations. In first approximation, we can account for this effect by assigning to the cantilevers an effective *dynamical* length ranging from their actual length, l , for small amplitude motions to $l + W/2$, for large ones. If we carry out the substitution $l \rightarrow l + W/2$ in $Q(\gamma, \beta_1)$ and reevaluate $\gamma_{1,2}$, we find $\gamma_{1,2} = 2.085115$ and a frequency

$f_{1,2} \simeq 1.55$ GHz, within 3 percent of the simulated value.

The shapes of the central beam predicted by the continuum model are the same for the fundamental and first collective modes. They are given by $Y_1(u)$, obtained from Eq. (33) for $\beta = \beta_1$. The shapes of the cantilever continua, however, are different and given by equation (29) as $H_{1,1}(u, v)$ and $H_{1,2}(u, v)$, respectively. A comparison of these results to those of the finite element simulation is done in Fig. 5. The FE and CM results for the fundamental and first collective modes are given in the upper left and upper right panel, respectively. As indicated, the FE result is to the right of the CM result. In both cases, the color code (online) indicates the displacement (amplitude) of the elements with respect to the clamps of the central beam (i.e. its extremities). For the CM results, only half of the absolute displacement of the cantilever continuum, $Y_1(u) + H_{1,k}(u, v)$, $k = 1, 2$, $v \geq 0$, is displayed. For $v = 0$, this displacement is precisely the beam's, $Y_1(u)$. As we see, the continuum model predictions are in excellent agreement with the finite element results. For both the fundamental and the first collective modes, the shape of the central beam is in the fundamental mode of a bare beam, $Y_1(u)$. In the fundamental mode, the deflection of the cantilever continuum with respect to the beam is imperceptible as predicted by the continuum model in the small γ limit (see III D). Indeed, from Eq. (43), we have $H_{1,1}(u, v) \propto \gamma_{1,1}^4 Y_1(u)$, which means that the continuum deflection is roughly 5000 times smaller than that of the beam. This is markedly different for the first collective mode where the motion of the continuum is on the order of the beam amplitude as seen on the upper right panel. Note that, if their amplitudes are very different, the actual shapes of the continua for the fundamental and first collective modes are similar and are given to a very good approximation by the fundamental mode of a bare cantilever. This somewhat surprising fact becomes clear on the modal expansion of the cantilever continuum, $H_{n,k}(u, v) \equiv \tilde{H}_{n,k}(v)Y_n(u)$. Introducing the normalized cantilever modes, $\psi_l(v)$, satisfying $\psi_l^{(iv)}(v) = \gamma_{\infty,l}^4 \psi_l(v)$, we obtain from Eq. (26)

$$\tilde{H}_{n,k}(v) = \sum_{l=1}^{\infty} \frac{\gamma_{n,k}^4 \Psi_l}{\gamma_{\infty,l}^4 - \gamma_{n,k}^4} \psi_l(v), \quad (58)$$

where $\Psi_l = \int_0^1 \psi_l(v) dv = -(2/\gamma)(\cos \gamma + \cosh \gamma)/(\sin \gamma + \sinh \gamma)$, where $\gamma = \gamma_{\infty,l}$. Now, we have seen in section III E that, for $k \geq 2$, $\gamma_{n,k}$ is very close to $\gamma_{\infty,k-1}$. According to Eq. (58), this means that the mode selected for the cantilever continuum is $\psi_{k-1}(v)$. In particular, for the first collective mode, $\gamma_{1,2}$, the continuum adopts basically the shape of the *fundamental* cantilever mode, $\psi_1(v)$. For the modes of the fundamental band ($k = 1$), this is also the fundamental cantilever mode that is predominantly excited, even if its amplitude is so small compared to the beam's that the cantilevers seem flat at the scale of the figure.

To analyze further the similarities between the FE and CM results, the first excited modes of the fundamen-

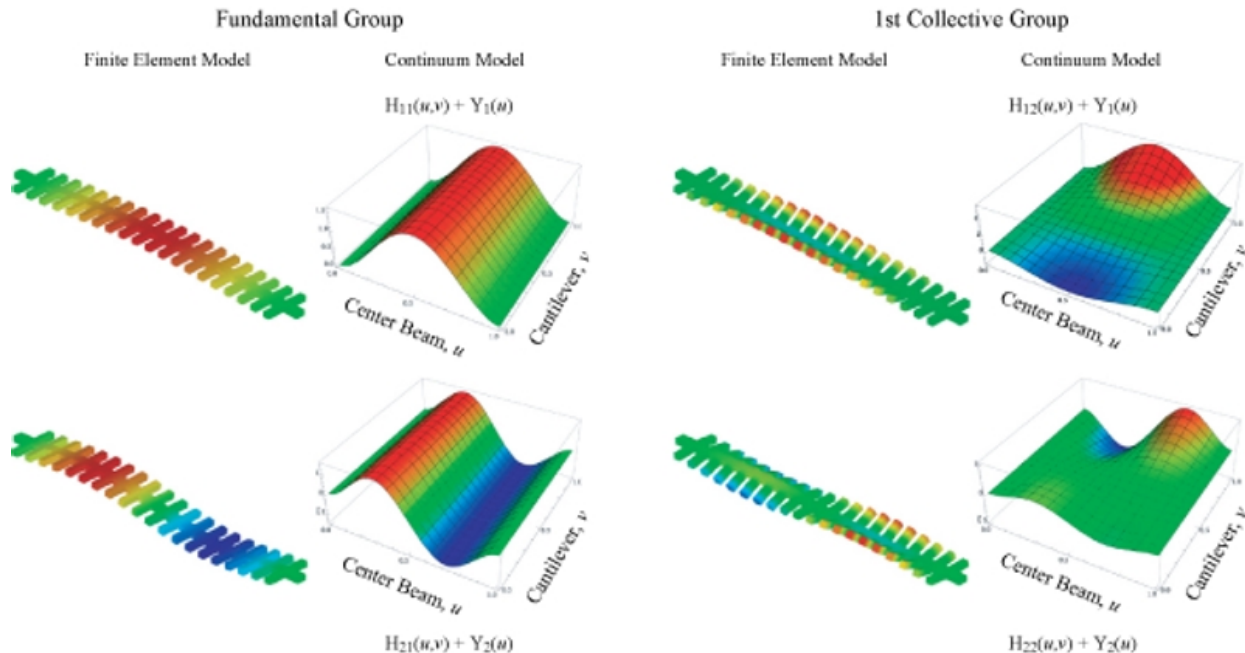


FIG. 5: Comparison between finite element (FE) and continuum model (CM) results for the fundamental mode (upper left panel), the first excited mode of the fundamental group (lower left panel), the first collective mode (upper right panel), and the first excited collective mode (lower right panel). The parameters for the antenna structure are those quoted in II A.

tal and collective bands are displayed in the lower left and right panels of Fig. 5, respectively. We clearly observe in both cases that the beam deflection is in the first excited mode of a bare beam, $Y_2(u)$, as predicted by the continuum model. Moreover, as for the fundamental mode, the cantilevers of the first excited mode of the fundamental group are hardly moving. Evaluating the first root of $Q(\gamma, \beta_2) = 0$ with $\beta_2 = 7.85320\dots$ yields $\gamma_{2,1} = 0.31114\dots$. This is small enough for the results of section III D to hold. Indeed, expression (41) gives $\gamma_{2,1} \simeq 0.31116\dots$. Therefore, the continuum deflection can safely be evaluated from Eq. (43) and we find that it is roughly 100 times smaller than the beam deflection, which explains that no cantilever motion can be detected in the FE results. Once again, this is markedly different for the first excited mode of the collective group whose cantilevers, according to the finite element results, are experiencing a deflection comparable to the beam amplitude in full agreement with the predictions of the continuum model. Note that for this two first excited modes of the fundamental and collective bands, the cantilever deflections adopt the shape of the fundamental mode of a bare cantilever, $\psi_1(v)$, as indicated by the modal expansion (58).

Even though one-dimensional in essence, the continuum model gives a good qualitative understanding of the modes of the 3D antenna. It correctly reproduces the modal shapes of the central beam and the cantilevers observed in the finite element simulation and is able to explain the frequency clustering occurring in the spectrum of the structure. We use it in the next section as the basic model in the investigation of the effect of a two-

frequency driving on the response of a weakly nonlinear and dissipative antenna.

H. Driven damped system: Exact solution

We conclude this section devoted to the linear system by calculating the exact solution of a damped antenna structure driven by a spatially uniform harmonic force density, $f(t)$, in the continuum approximation. This force density can, for instance, be exerted by an external magnetic field, B , orthogonal to the flexural vibrations of the central beam, acting on an ac-current with frequency ω_d passed through the thin layer of gold coating the structure. The beam vibrations then generate in turn an electromotive voltage $V_{emf}(t)$ at the clamped ends of the antenna that is proportional to the rate of change of the magnetic flux,

$$V_{emf}(t) = B \int_0^L \frac{\partial y(x, t)}{\partial t} dx. \quad (59)$$

Ultimately, this voltage can be monitored to determine the motion of the central beam of the structure and to derive its “spectrum” i.e., the time root-mean-square of the induced voltage, $\sqrt{\langle V_{emf}^2(t) \rangle}$, versus the driving frequency, ω_d . This detection scheme has been used in the previously reported experimental measurements of the antenna resonators in Ref. [12, 21]. Other activation/detection schemes such as electrostatic, piezoelectric, and optical are typically also sensitive to the av-

erage transverse displacement of resonating elements, and the following analysis applies quite generally.

1. Model

Supplementing the equations of motion (18)-(19) with damping and driving terms we obtain

$$\mathcal{E}_b \frac{\partial^4 y}{\partial x^4} + \mu_b \frac{\partial^2 y}{\partial t^2} + \nu_b \frac{\partial y}{\partial t} = -\frac{2\mathcal{E}_t N}{L} \frac{\partial^3 \eta}{\partial \xi^3} \Big|_{\xi=0} + f(t) \quad (60)$$

$$\mathcal{E}_t \frac{\partial^4 \eta}{\partial \xi^4} + \mu_t \frac{\partial^2 \eta}{\partial t^2} + \nu_t \frac{\partial \eta}{\partial t} = -\mu_t \frac{\partial^2 y}{\partial t^2} - \nu_t \frac{\partial y}{\partial t}. \quad (61)$$

Boundary conditions for the beam and cantilever deflections are the same as in (20) and (21). The harmonic force density is given by $f(t) = f \cos(\omega_d t)$. Note that in Eq. (61), the damping term affecting the cantilevers involves their absolute displacement, $y(x, t) + \eta(x, \xi, t)$, rather than their relative displacement, $\eta(x, \xi, t)$. The choice of an appropriate damping term depends of course on the type of damping experienced by the structure. To simplify, we consider here that damping occurs through air friction and is then proportional to the absolute velocity of the cantilevers. Moreover, it is proportional to the surface in contact with the ambient air. For that reason, the damping per unit length is proportional to the width of the element involved and then $\nu_t/\nu_b = w/W = \mu_t/\mu_b = \mathcal{E}_t/\mathcal{E}_b$. Material damping, whether of the viscoelastic or hysteretic type (see for instance Ref. [24]), would essentially affect the rigidities of Eqs. (60) and (61) in such a way that \mathcal{E} is replaced by $\mathcal{E} + \mathcal{E}^* \partial/\partial t$. The exact solution of system (60)-(61) can still be obtained in this case.

2. Exact solution

Introducing the Fourier transform $\tilde{g}(\omega) = \int dt e^{i\omega t} g(t)$ and its inverse $g(t) = \int d\omega e^{-i\omega t} \tilde{g}(\omega)/(2\pi)$ and using the dimensionless quantities defined in (11), we can cast Eqs. (60)-(61) into

$$\frac{\partial^4 \tilde{y}}{\partial u^4} - \mu_c^4 \tilde{y} = -NR \frac{\partial^3 \tilde{\eta}}{\partial v^3} \Big|_{v=0} + \tilde{F}(\omega), \quad (62)$$

$$\frac{\partial^4 \tilde{\eta}}{\partial v^4} - \gamma_c^4 \tilde{\eta} = \gamma_c^4 \tilde{y}, \quad (63)$$

where $F(t) = F \cos(\omega_d t)$ with $F = L^4 f/\mathcal{E}_b$ and

$$\begin{aligned} \gamma_c^4 &= \frac{l^4}{\mathcal{E}_t} (\mu_t \omega^2 + i\nu_t \omega), \\ \mu_c^4 &= \frac{L^4}{\mathcal{E}_b} (\mu_b \omega^2 + i\nu_b \omega) = \left(\frac{L\gamma_c}{l} \right)^4. \end{aligned} \quad (64)$$

These last parameters are the complex version (because of the presence of damping) of the parameters μ and γ defined in (11). Note also that F has the dimension of a

length. As in the earlier case, we can solve Eq. (63) with its boundary conditions:

$$\tilde{\eta}(u, v, \omega) = \tilde{H}(v, \omega) \tilde{y}(u, \omega), \quad (65)$$

where

$$\begin{aligned} \tilde{H}(v, \omega) &= [A_1(\gamma_c) \cos(\gamma_c v) + A_2(\gamma_c) \sin(\gamma_c v) \\ &+ A_3(\gamma_c) \cosh(\gamma_c v) + A_4(\gamma_c) \sinh(\gamma_c v) - 1]. \end{aligned} \quad (66)$$

The coefficients A_i are the same as those given in (30). Reinstating this expression in Eq. (62), we finally obtain

$$\frac{\partial^4 \tilde{y}(u, \omega)}{\partial u^4} - \beta_c^4 \tilde{y}(u, \omega) = \tilde{F}(\omega), \quad (67)$$

where

$$\beta_c^4 = \mu_c^4 + \gamma_c^3 RN \frac{\cos \gamma_c \sinh \gamma_c + \sin \gamma_c \cosh \gamma_c}{1 + \cos \gamma_c \cosh \gamma_c}, \quad (68)$$

which is the complex analog of the secular equation (32). Finally, applying the appropriate boundary conditions to $\tilde{y}(u, \omega)$ we can, after some algebra, cast the solution to Eq. (67) into

$$\begin{aligned} \tilde{y}(u, \omega) &= \left\{ T(\beta_c) \left[\frac{\cos(\beta_c(u-1/2))}{\sin(\beta_c/2)} + \right. \right. \\ &\quad \left. \left. + \frac{\cosh(\beta_c(u-1/2))}{\sinh(\beta_c/2)} \right] - 1 \right\} \frac{\tilde{F}(\omega)}{\beta_c^4}, \end{aligned} \quad (69)$$

where we have defined

$$T(\beta_c) = \frac{\tan(\beta_c/2) \tanh(\beta_c/2)}{\tan(\beta_c/2) + \tanh(\beta_c/2)}. \quad (70)$$

Now, the driving $f(t)$ being harmonic, we have $\tilde{F}(\omega) = F\pi[\delta(\omega-\omega_d) + \delta(\omega+\omega_d)]$. Noticing that the sign inversion $\omega \rightarrow -\omega$ amounts to taking the complex conjugate, we can finally show:

$$y(x, t) = F \text{Re}\{\exp(-i\omega_d t) \tilde{y}_h(u, \omega_d)\}, \quad (71)$$

where $\tilde{y}_h(u, \omega) = \tilde{y}(u, \omega)/\tilde{F}(\omega)$. Then

$$\begin{aligned} y(x, t) &= F \text{Re} \left\{ \frac{e^{-i\omega_d t}}{\beta_c^4} \left[T(\beta_c) \left(\frac{\cos(\beta_c(u-1/2))}{\sin(\beta_c/2)} + \right. \right. \right. \\ &\quad \left. \left. \left. + \frac{\cosh(\beta_c(u-1/2))}{\sinh(\beta_c/2)} \right) - 1 \right] \right\}. \end{aligned} \quad (72)$$

Expression (69) makes it clear that the shape of the central beam induced by the force density $f(t)$ is symmetric with respect to its midpoint, $u = 1/2$. This is expected as the force density itself possesses this symmetry. Consequently, none of the antisymmetric modes of the central beam are excited by this method. Moreover, in presence of dissipation, the beam shape never corresponds to an exact symmetric modal shape even when the driving frequency is one of the structure modal frequencies. We can see that for weak dissipation, however, the denominator of $T(\beta_c)$ becomes small (on the order of ν_t) when $\omega_d \sim \omega_{2n+1, k}$. This is because the solutions to $\tan(x/2) + \tanh(x/2) = 0$ are precisely the β_{2n+1} 's. This eventually leads $y(x, t)$ to assume a shape close to the mode $Y_{2n+1}(u)$.

3. Modal expansion

As we have seen earlier, the modes of the antenna structure are such that the central beam possesses the *exact* shape of a clamped-clamped mode, $Y_n(u)$ (see Eq. (33)). However, the force $f(t)$ applied to the beam excites now *all* symmetric clamped-clamped modes. To get a sense of which modes are predominantly excited, we first expand the Fourier transform of the deflection as $\tilde{y}(u, \omega) = \sum_n \tilde{y}_n(\omega) Y_n(u)$, insert it in Eq. (67) and solve for $\tilde{y}_n(\omega)$. The beam deflection given by Eq. (71) then reads

$$y(x, t) = F \sum_{n=0}^{\infty} \frac{\Gamma_{2n+1} \cos(\omega_d t + \vartheta_{2n+1}(\omega_d))}{|\beta_c^4(\omega_d) - \beta_{2n+1}^4|} Y_{2n+1}(u), \quad (73)$$

where $\Gamma_n = \int_0^1 Y_n(u) du$ and where $\vartheta_n(\omega) = \arg(\beta_c^4(\omega) - \beta_n^4)$. The reason why the sum runs exclusively over odd numbers in Eq. (73) is because integrals of antisymmetric clamped-clamped modes, Γ_{2n} , vanish which confirms that none of them is excited by $f(t)$. For symmetric modes, a simple calculation yields $\Gamma_{2n+1} = 4 \tan(\beta_{2n+1}/2)/\beta_{2n+1}$. Clearly, expression (73) shows that the mode $Y_{2n+1}(u)$ is singled out when the driving frequency is close to one of the modal frequencies $\omega_{2n+1,k}$ and the dissipation is weak enough ($|\beta_c^4(\omega_d) - \beta_{2n+1}^4| \propto \nu_t$ in this case, see III H 5).

Also of interest is the modal expansion of the cantilever continuum. Introducing the normalized cantilever modes, $\psi_k(v)$, $k \geq 1$, satisfying $\psi_k^{(iv)}(v) = \gamma_{\infty,k}^4 \psi_k(v)$, we can expand $\tilde{H}(v, \omega)$ in (66) as $\tilde{H}(v, \omega) = \sum_k \tilde{H}_k(\omega) \psi_k(v)$, uses Eq. (65) and insert it in Eq. (63), and finally solve for $\tilde{H}_k(\omega)$. This yields

$$\tilde{H}(v, \omega) = \sum_{k=1}^{\infty} \frac{\gamma_c^4(\omega) \Psi_k}{\gamma_{\infty,k}^4 - \gamma_c^4(\omega)} \psi_k(v), \quad (74)$$

where $\Psi_k = \int_0^1 \psi_k(v) dv = -(2/\gamma)(\cos \gamma + \cosh \gamma)/(\sin \gamma + \sinh \gamma)$, where $\gamma = \gamma_{\infty,k}$. Hence, $\Psi_k \simeq -2/\gamma_{\infty,k}$, as k becomes large. The interesting point about this calculation is to show what cantilever mode is selected according to the driving frequency. When the latter is close to the modal frequency $\omega_{n,k}$ with n small, and provided the dissipation is weak enough, $\gamma_c(\omega_{n,k}) \simeq \gamma_{n,k}$. Now, we have seen in section III E that, for $k \geq 2$, $\gamma_{n,k}$ is very close to $\gamma_{\infty,k-1}$. According to Eq. (74), this means that for $\omega_d \sim \omega_{n,k}$, the mode selected for the cantilever continuum is $\psi_{k-1}(v)$. In particular, if the system is driven near the first *collective* mode frequency, $\omega_{1,2}$, the continuum adopts basically the shape of the *fundamental* cantilever mode. Note that, for driving frequencies in the fundamental band ($k = 1$), this is always the fundamental cantilever mode that is predominantly excited. For other bands ($k \geq 2$), the continuum interpolates between the shape of the mode $\psi_{k-1}(v)$ close to the lower band edge and $\psi_k(v)$ close to the upper band edge. In practice, however, as our model provides consistent results for $n < N$ only, the range of physically relevant frequencies is restricted to the lower band edge. For all peaks but those

of the fundamental band, therefore, the relevant modes of the structure at frequency $\omega_{n,k}$ are $Y_n(u)$ and $\psi_{k-1}(v)$.

4. Amplitude-frequency spectrum

Most of the time, this is not the beam deflection $y(x, t)$ but rather its average over the beam length (or its time-derivative, see below) that is detected. For that reason, we define

$$\bar{y}(t) \equiv \frac{1}{L} \int_0^L y(x, t) dx. \quad (75)$$

Using expression (72), we immediately obtain

$$\bar{y}(t) = \mathcal{A}(\omega_d) \cos(\omega_d t - \theta(\omega_d)), \quad (76)$$

where the amplitude $\mathcal{A}(\omega)$ and the phase $\theta(\omega)$ are respectively given by

$$\begin{aligned} \mathcal{A}(\omega) &= \frac{F}{|\beta_c^4|} \left| \frac{4T(\beta_c)}{\beta_c} - 1 \right|, \\ \theta(\omega) &= \arg \left(\frac{1}{\beta_c^4} \left[\frac{4T(\beta_c)}{\beta_c} - 1 \right] \right). \end{aligned} \quad (77)$$

Fig. 6(a) displays the amplitude-frequency spectrum for the antenna parameters given in II A. Quantities plotted are the dimensionless amplitude, $\mathcal{A}(\omega)/F$, given by Eq. (77), versus the dimensionless frequency $\omega/\omega_{1,1}$. Therefore, the peak of the fundamental is located at 1. The peak of the first collective mode (first frequency of the second band) is approximately located at $\omega_{1,2}/\omega_{1,1} = 119.23$ as seen on Fig. 6(b). The dissipation parameter has been chosen in such a way as to provide a fundamental peak with quality factor $Q = \mu_t \omega_{1,1}/\nu_t$ on the order of $\sim 10^3$, a typical value in experiments. The physically relevant part of the spectrum (corresponding to $n < N$, that is $|\beta_c(\omega)| < (N + 1/2)\pi$), is drawn in solid line while the irrelevant part is drawn in dotted line. Because of the weak damping, frequency peaks occur when the driving frequency is close to one of the modal frequencies, $\omega_{2n+1,k}$. As seen in Fig. 6(a), peak amplitudes decrease rapidly as the frequency increases within a given band. But the first peak of the collective band, approximately located at $\omega_{2,1} \simeq 119.23 \omega_{1,1}$, is much higher than the last peaks of the fundamental band. That is why it is easily observed in experiments. An analytical formula for peak heights is obtained in the next section in the weakly dissipative regime.

Also of interest are the dips occurring slightly before the peaks. Their occurrence is due to the fact that at certain frequencies, the integral of the shape of the central beam over its length is close to zero. This is especially important for detection schemes involving an electromotive voltage because the signal is close to zero in this case. For a *non-dissipative system*, there are frequencies such that the integral is exactly zero. The shape of the central beam resembles the modal shapes $Y_{2n+1}(u)$, $n \geq 1$, in

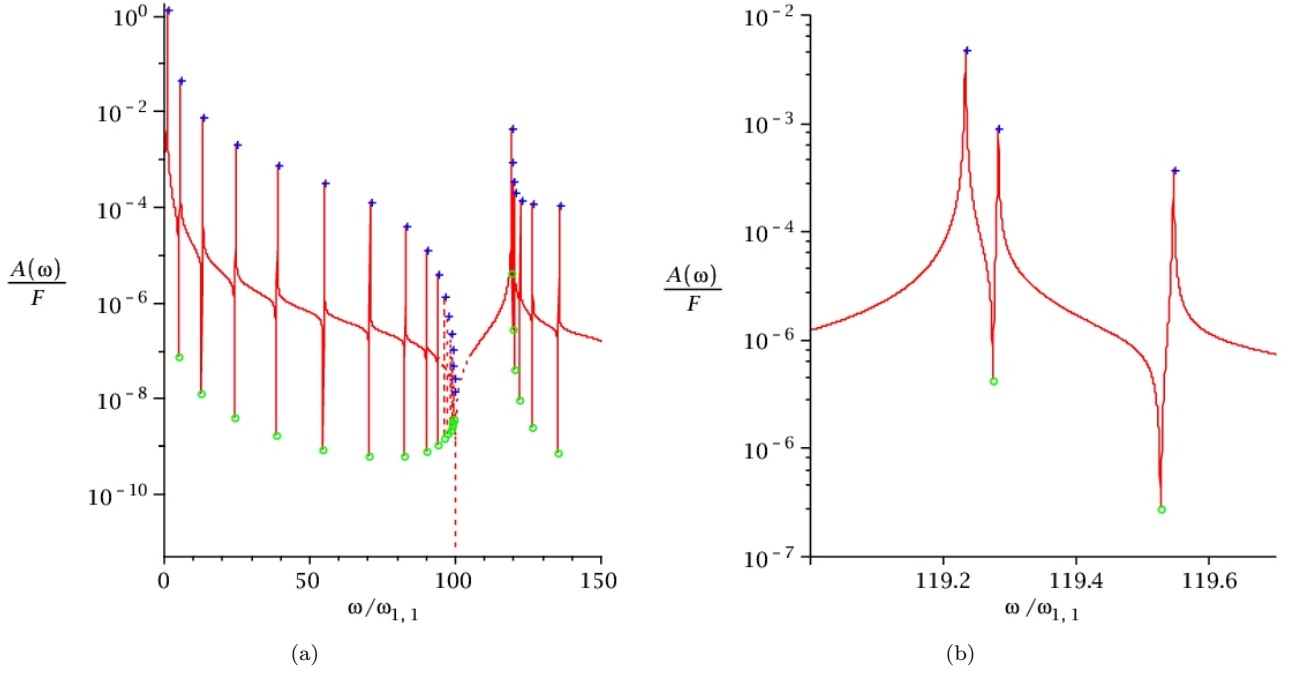


FIG. 6: (a): Amplitude-Frequency spectrum, $(\mathcal{A}(\omega)/F)$ versus $\omega/\omega_{1,1}$, obtained from Eq. (77) for $N = 20$ and the antenna parameters given in II A. Solid lines correspond to $n < N$ (physically relevant frequencies) and the dotted one to $n > N$. (b): Zoom in the region of the 1st collective frequency peak. For both (a) and (b), analytical results for peaks (+) and dips (o) are obtained from Eqs. (80) and (81), respectively.

this case. From Eq. (77), we see that spectral dips are given by the simple relation $4T(\beta) = \beta$, where $T(\beta)$ is given in (70). Denoting with a hat all quantities related to the dips, we can show that the solution of the previous equation reads approximately

$$\hat{\beta}_{2n+1} \simeq \beta_{2n+1} + \frac{4}{4 - \beta_{2n+1}}, \quad n \geq 1. \quad (78)$$

This explains why dips are close to the frequency peaks. The corresponding frequencies are obtained by solving the secular equation $Q(\gamma, \hat{\beta}_{2n+1}) = 0$ for γ (see Eq. (35)) whose solutions $\hat{\gamma}_{2n+1,k}$ define $\hat{\omega}_{2n+1,k} = \sqrt{\mathcal{E}_t/\mu_t (\hat{\gamma}_{2n+1,k}/l)^2}$. Last, the deepest dip occurring around 100 in Fig. 6(a) is due to the upper band edge of the fundamental band, obtained in the non dissipative case for $\omega_{\infty,1}/\omega_{1,1} = (\gamma_{\infty,1}/\gamma_{1,1})^2 \simeq 100.103$. Though, this part of the spectrum is not physically relevant.

5. Weak dissipation

Analytical results for weakly dissipative systems are obtained by expanding the quantities of interest around their value in absence of dissipation ($\nu_t = 0$). Let us assume that, for $\nu_t = 0$, ω_0 is the frequency of interest, a modal or dip frequency, for example. Then $\gamma_0 = l(\mu_t \omega_0^2/\mathcal{E}_t)^{1/4}$ and β_0 given by (32) are real. For $\omega \sim \omega_0$, we have $\beta_c^4(\omega, \nu_t) \simeq \beta_0^4 + [(\omega - \omega_0) \partial \gamma_c^4/\partial \omega|_0 + \nu_t \partial \gamma_c^4/\partial \nu_t|_0] \partial \beta_c^4/\partial \gamma_c^4|_0$. Now, using Eq. (68) for β_c , Eq.

(64) for γ_c and the result obtained in (52) yields

$$|\beta_c^4(\omega) - \beta_0^4| \simeq \frac{L^4 \mu_t}{\mathcal{E}_t} \left[1 + \frac{2Nm_t}{m_b} L(\gamma_0) \right] \times \sqrt{4\omega_0^2 (\omega - \omega_0)^2 + \left(\frac{\nu_t \omega_0}{\mu_t} \right)^2}, \quad (\omega \sim \omega_0) \quad (79)$$

Notice that, because $\omega \sim \omega_0$, the function under the square root is, in first order in ν_t , equivalent to $(\omega^2 - \omega_0^2)^2 + (\nu_t \omega/\mu_t)^2$, which is the typical form for a harmonic oscillator. But $\beta_c(\omega, \nu_t)$ has to be expanded up to second order in ν_t and $\omega - \omega_0$ to compute the correct frequency shift induced by the damping because the latter is of order ν_t^2 .

By expanding $\beta_c(\omega)$ around β_{2n+1} and using Eq. (77), we find that the amplitude of the peak with frequency $\omega_{2n+1,k}$ is given by $\mathcal{A}(\omega) \simeq 16F \tanh^2(\beta_{2n+1}/2)/(\beta_{2n+1}^2 |\beta_c^4(\omega) - \beta_{2n+1}^4|)$. Therefore, from Eq. (79) we obtain the peak height as

$$\mathcal{A}_{m,k}^{\text{peak}} \simeq \frac{16\mathcal{E}_t F}{L^4 \nu_t} \left[1 + \frac{2Nm_t}{m_b} L(\gamma_{m,k}) \right]^{-1} \frac{\tanh^2\left(\frac{\beta_m}{2}\right)}{\beta_m^2 \omega_{m,k}}. \quad (80)$$

where $m = 2n + 1$, $n \geq 0$. In the same way, expanding $\beta_c(\omega)$ around $\hat{\beta}_{2n+1}$ (see Eq. (78)) we can show after some algebra that the amplitude of a dip with frequency $\hat{\omega}_{2n+1,k}$ is given by $\mathcal{A}(\omega) \simeq \frac{F}{4\hat{\beta}_{2n+1}^8} \left[\frac{\hat{\beta}_{2n+1}/2}{\tanh(\hat{\beta}_{2n+1}/2)} - 1 \right]^2 |\beta_c^4(\omega) - \hat{\beta}_{2n+1}^4|$. Hence, the

minimum of the dip

$$\mathcal{A}_{m,k}^{\text{dip}} \simeq \frac{FL^4\nu_t}{4\mathcal{E}_t} \left(\frac{\hat{\beta}_m/2}{\tanh(\hat{\beta}_m/2)} - 1 \right)^2 \times \left[1 + \frac{2Nm_t}{m_b} L(\gamma_{m,k}) \right] \frac{\hat{\omega}_{m,k}}{\hat{\beta}_m^8}, \quad (81)$$

with $m = 2n + 1$, $n \geq 1$.

6. Electromotive potential spectrum

From Eqs. (75) and (76), it is now straightforward to evaluate the electromotive potential $V_{emf}(t)$ given in Eq. (59). It reads

$$\frac{V_{emf}(t)}{LB} = \frac{d\bar{y}(t)}{dt} = \omega_d \mathcal{A}(\omega_d) \sin(\omega_d t - \theta(\omega_d) - \pi), \quad (82)$$

from which we eventually deduce the time r.m.s.

$$\sigma_{emf} \equiv \sqrt{\langle V_{emf}^2(t) \rangle} = \frac{BFL\omega_d}{\sqrt{2}} \frac{1}{|\beta_{c,d}^4|} \left| \frac{4T(\beta_{c,d})}{\beta_{c,d}} - 1 \right|. \quad (83)$$

From the formulas of the previous section we can evaluate the peak maxima and dip minima of the electromotive r.m.s. and we are able to compare them with those observed in experiments.

IV. NONLINEAR SYSTEM DRIVEN BY TWO FREQUENCIES

It has been observed experimentally [28] that, if in addition to being driven at the frequency of the fundamental mode the antenna is also driven at the frequency of the collective mode, the frequency peak of the fundamental mode experiences a slight shift. This frequency shift is the signature of a modal coupling that occurs because of the presence of nonlinearity and dissipation in the system [27]. To explain the interaction of these two widely spaced modes, we investigate the effect of a two-frequency driving on the response of a weakly nonlinear and dissipative antenna. We supplement the equations of motion of our continuum model, Eqs. (18) and (19), with nonlinear terms that take into account the possible material and geometrical nonlinearities of the structure and with damping terms proportional to the transverse velocity of the elements. These terms, small compared to the amplitude of vibration of the antenna, are treated within the Lagrangian approach described in [27] to derive the frequency-amplitude relation of the model.

A. Lagrangian approach

In the previous section, we solved the linear continuum model exactly and found its modes, $\varphi_{n,k} =$

$(y_n(x, t), \eta_{n,k}(x, \xi, t))^T$, to be related to two parameters: β_n , root of $\cos \beta \cosh \beta = 1$ and $\gamma_{n,k}$, solution to Eq. (32) or (35). The frequency $\omega_{n,k}$ of $\varphi_{n,k}$ is determined by Eq. (36) and its modal shape derived from Eqs. (29) and (33). In particular, the fundamental mode is given by the parameters $(\beta_1, \gamma_{1,1})$ and the collective mode we are interested in by the parameters $(\beta_1, \gamma_{1,2})$. For clarity in the notations, we rename these two modes $\varphi_1 = (y_1(x, t), \eta_1(x, \xi, t))^T$ and $\varphi_2 = (y_2(x, t), \eta_2(x, \xi, t))^T$, respectively and denote their respective frequencies by ω_1 and ω_2 where

$$\omega_i = \sqrt{\frac{\mathcal{E}_t}{\mu_t}} \left(\frac{\gamma_{1,i}}{l} \right)^2, \quad i \in \{1, 2\}. \quad (84)$$

It is observed experimentally that φ_1 and φ_2 are coupled in the sense that the amplitude-frequency curve (resonance) of the fundamental mode is modified when the higher mode is driven. This coupling is attributed to the presence of nonlinearities in the antenna. To explain this phenomenon, we treat the nonlinearities and the damping affecting the system as a perturbation of the fundamental and collective modes, φ_1 and φ_2 . These perturbative terms are responsible for a modulation of the linear modes that we evaluate by a multiple scale method. Hereafter, we closely follow the Lagrangian approach of Ref. [27] because it offers a particularly suitable framework to derive the modulation equations.

When the driving amplitude (or power) is small enough, the solution $\varphi = (y(x, t), \eta(x, \xi, t))^T$ to the nonlinear equations of motion is, to a good approximation, given by a superposition of φ_1 and φ_2 with slowly modulated amplitudes. Following the multiple scale approach, we write it as $\varphi = A_1\varphi_1 + A_2\varphi_2$, that is

$$\begin{aligned} \begin{pmatrix} y(x, t) \\ \eta(x, \xi, t) \end{pmatrix} = \varepsilon \left\{ A_1(T_2) Y_1(u) e^{i\omega_1 T_0} \begin{pmatrix} 1 \\ H_1(v) \end{pmatrix} + \right. \\ \left. + A_2(T_2) Y_1(u) e^{i\omega_2 T_0} \begin{pmatrix} 1 \\ H_2(v) \end{pmatrix} + c.c. \right\} \quad (85) \end{aligned}$$

In this expression, $c.c.$ denotes the complex conjugate, ε is a small bookkeeping parameter, $H_i(v) = \tilde{H}_{1,i}(v)$ where \tilde{H} is defined in Eq. (29) and, according to the multiple scale method, we have introduced two time scales, $T_0 = t$ and $T_2 = \varepsilon^2 t$. The Lagrangian of our system is given by

$$\begin{aligned} \mathcal{L} = \int_0^L dx \left[\frac{\mu_b}{2} \left(\frac{\partial y}{\partial t} \right)^2 - \frac{\mathcal{E}_b}{2} \left(\frac{\partial^2 y}{\partial x^2} \right)^2 \right] + \\ + \frac{2N}{L} \int_0^L dx \int_0^l d\xi \left[\frac{\mu_t}{2} \left(\frac{\partial \eta}{\partial t} + \frac{\partial y}{\partial t} \right)^2 - \frac{\mathcal{E}_t}{2} \left(\frac{\partial^2 \eta}{\partial \xi^2} \right)^2 \right] + \\ + (\text{NLT}) + F_1 \cos(\Omega t) \int_0^L y dx + F_2 \cos(\omega t) \int_0^L y dx, \quad (86) \end{aligned}$$

where (NLT) stands for ‘‘NonLinear Terms’’. To express the fact that the driving frequencies, Ω and ω , are close

to the linear frequencies of the fundamental and excited modes, we write them as

$$\Omega = \omega_1 + \varepsilon^2 \sigma_1 \quad ; \quad \omega = \omega_2 + \varepsilon^2 \sigma_2. \quad (87)$$

To describe the nonlinear response of the cantilevers and the central beam, neglecting the effects of rotatory inertia and shear deformations, we add the following nonlinear terms to the Lagrangian [27]

$$\begin{aligned} \text{NLT} = & \int_0^L dx \left\{ \frac{\mu_b}{8} \left[\frac{\partial}{\partial t} \int_0^x \left(\frac{\partial y}{\partial x'} \right)^2 dx' \right]^2 - \frac{\mathcal{E}_b}{2} \left(\frac{\partial y}{\partial x} \frac{\partial^2 y}{\partial x^2} \right)^2 \right\} + \\ & \frac{2N}{L} \int_0^L dx \int_0^l d\xi \left\{ \frac{\mu_t}{8} \left[\frac{\partial}{\partial t} \int_0^\xi \left(\frac{\partial \eta}{\partial \xi'} \right)^2 d\xi' \right]^2 - \frac{\mathcal{E}_t}{2} \left(\frac{\partial \eta}{\partial \xi} \frac{\partial^2 \eta}{\partial \xi^2} \right)^2 \right\}. \end{aligned} \quad (88)$$

Finally, we take into account the damping effects of the viscous forces acting on the antenna through the virtual work

$$\begin{aligned} \delta W = & - \int_0^L dx C_y \frac{\partial y}{\partial t} \delta y \\ & - \frac{2N}{L} \int_0^L dx \int_0^l d\xi C_\eta \left(\frac{\partial y}{\partial t} + \frac{\partial \eta}{\partial t} \right) \delta \eta, \end{aligned} \quad (89)$$

where C_y and C_η are the viscosities of the beam and the cantilevers, respectively.

To account for the fact that damping effects and driving forces are of the same order of magnitude as the nonlinear effects, we scale the viscosities as $C_y = \varepsilon^2 c_y$ and $C_\eta = \varepsilon^2 c_\eta$ and the forces as $F_j = \varepsilon^3 f_j$, $j = 1, 2$. We now proceed as explained in Ref. [27] to derive a time-averaged Lagrangian from Eqs. (85), (86) and (88). We substitute (85) into the Lagrangian (86) and also into the virtual work (89), perform the spatial integrations and keep the slowly varying terms only - i.e. those that are either constant or function of T_2 only. This yields:

$$\begin{aligned} \frac{\langle \mathcal{L} \rangle}{\varepsilon^4} = & \sum_{j=1}^2 \{ i M_j \omega_j (A_j \bar{A}'_j - A'_j \bar{A}_j) + C_{jj} |A_j|^4 + \\ & + \mathcal{F}_j (\bar{A}_j e^{i\sigma_j T_2} + cc) \} + 2C_{12} |A_1|^2 |A_2|^2 \end{aligned} \quad (90)$$

$$\frac{\langle \delta W \rangle}{\varepsilon^4} = \sum_{j=1}^2 Q_j \delta A_j + cc, \quad \text{with} \quad Q_j = 2i\omega_j \mu_j \bar{A}_j, \quad (91)$$

where

$$\begin{aligned} M_j &= m_b + 2N m_t L_{jj} \quad ; \quad \mathcal{F}_j = \frac{L}{2} f_j \Gamma_4 \\ \mu_j &= \frac{1}{2} (L c_y + 2N l c_\eta \Lambda_{jj}) \\ C_{jj} &= \frac{\Gamma_1 m_b \omega_j^2}{L^2} - \frac{3\Gamma_2 \mathcal{E}_b}{L^5} + \frac{2N\Gamma_3}{l^2} \left[m_t \omega_j^2 I_{jj} - \frac{3\mathcal{E}_t}{l^3} K_{jjj} \right] \\ C_{12} &= \frac{\Gamma_1 m_b (\omega_1^2 + \omega_2^2)}{L^2} - \frac{6\Gamma_2 \mathcal{E}_b}{L^5} + \frac{2N\Gamma_3}{l^2} \left[m_t (\omega_1^2 + \omega_2^2) I_{12} \right. \\ & \quad \left. - \frac{\mathcal{E}_t}{l^3} (K_{1122} + K_{2211} + 4K_{1212}) \right] \end{aligned} \quad (92)$$

and where

$$\begin{aligned} \Gamma_1 &= \int_0^1 \left(\int_0^u [Y_1'(\nu)]^2 d\nu \right)^2 du, \\ \Gamma_2 &= \int_0^1 [Y_1'(u) Y_1''(u)]^2 du, \\ \Gamma_3 &= \int_0^1 Y_1^4(u) du, \\ \Gamma_4 &= \int_0^1 Y_1(u) du, \\ L_{ij} &= \int_0^1 h_i(v) h_j(v) dv, \\ \Lambda_{ij} &= \int_0^1 h_i(v) (h_j(v) - 1) dv, \\ I_{ij} &= \int_0^1 \left(\int_0^v h_i'(\nu) h_j'(\nu) d\nu \right)^2 dv, \\ K_{ijkl} &= \int_0^1 h_i'(v) h_j'(v) h_k''(v) h_l''(v) dv. \end{aligned} \quad (93)$$

with $h_j(v) \equiv H_j(v) + 1$. A numerical/analytical evaluation of the above quantities for the antenna dimensions given in II A is provided in appendix C.

B. Modulation equations

Applying the extended Hamilton principle (see Ref. [27]), we obtain the equations of motion for the modulations $A_1(T_2)$ and $A_2(T_2)$ as

$$\frac{d}{dT_2} \left(\frac{\partial \mathcal{L}}{\partial \dot{A}_i} \right) = \frac{\partial \mathcal{L}}{\partial A_i} + \bar{Q}_i, \quad i \in \{1, 2\}. \quad (94)$$

From Eqs. (90) and (91), we then derive the following pair of modulation equations

$$\begin{aligned} 2i\omega_i (M_i A_i' + \mu_i A_i) = & -2A_i (C_{ii} |A_i|^2 + \\ & + C_{12} |A_j|^2) + \mathcal{F}_i e^{i\sigma_i T_2}, \end{aligned} \quad (95)$$

where $(i, j) \in \{1, 2\}$, $i \neq j$. Looking for solutions in the polar form

$$A_i(T_2) = \frac{1}{2} a_i(T_2) e^{i(\sigma_i T_2 - \theta_i(T_2))}, \quad i \in \{1, 2\}, \quad (96)$$

and separating the real and imaginary components of Eqs. (95), yields

$$\begin{aligned}\omega_i(\sigma_i - \theta'_i)M_i a_i &= \frac{a_i}{4} (C_{ii} a_i^2 + C_{12} a_j^2) - \mathcal{F}_i \cos(\theta_i), \\ \omega_i(M_i a'_i + \mu_i a_i) &= \mathcal{F}_i \sin(\theta_i).\end{aligned}\quad (97)$$

Looking for steady state (periodic) solutions, we impose $a'_j = 0$ and $\theta'_j = 0$ and we finally obtain the frequency-amplitude relations as

$$\sigma_1 = \frac{1}{4M_1\omega_1} [C_{11} a_1^2 + C_{12} a_2^2] \pm \sqrt{\frac{\mathcal{F}_1^2}{M_1^2\omega_1^2 a_1^2} - \frac{\mu_1^2}{M_1^2}}, \quad (98)$$

$$\sigma_2 = \frac{1}{4M_2\omega_2} [C_{22} a_2^2 + C_{12} a_1^2] \pm \sqrt{\frac{\mathcal{F}_2^2}{M_2^2\omega_2^2 a_2^2} - \frac{\mu_2^2}{M_2^2}}. \quad (99)$$

together with

$$\tan \theta_i = \frac{4\mu_i\omega_i}{C_{ii} a_i^2 + C_{12} a_j^2 - 4M_i\omega_i\sigma_i}, \quad i \neq j. \quad (100)$$

In first approximation the steady state solution can be cast into the form

$$\begin{aligned}\begin{pmatrix} y(x, t) \\ \eta(x, \xi, t) \end{pmatrix} &= Y_1(u) \left\{ a_1 \begin{pmatrix} 1 \\ H_1(v) \end{pmatrix} \cos(\Omega t - \theta_1) + \right. \\ &\quad \left. + a_2 \begin{pmatrix} 1 \\ H_2(v) \end{pmatrix} \cos(\omega t - \theta_2) \right\}. \quad (101)\end{aligned}$$

The amplitudes a_1 and a_2 are assumed small enough for the perturbation expansion to hold (notice that the book-keeping parameter ε has been absorbed in the amplitudes and that Eqs. (98)-(99) can be used as such provided the detunings σ_j are redefined as $\sigma_j \equiv \varepsilon^2 \sigma_j$, the viscosities μ_j as $\mu_j \equiv \varepsilon^2 \mu_j$ and the forces \mathcal{F}_j as $\mathcal{F}_j \equiv \varepsilon^3 \mathcal{F}_j$).

C. Discussion

The frequency-amplitude relations (98)-(99) allow us to evaluate the frequency shift of the fundamental peak induced by a driving of the higher mode at the exact linear resonance frequency, ω_2 . This frequency shift is determined as the difference between the maximum of the resonance peak of the fundamental mode and ω_1 . Now, the amplitude a_1 becomes maximum if the square root in the r.h.s. of (98) vanishes, that is,

$$a_1^{\max} = \left| \frac{\mathcal{F}_1}{\mu_1\omega_1} \right|. \quad (102)$$

For a system whose higher mode is driven exactly at frequency $\omega = \omega_2$ we have of course $\sigma_2 = 0$ and then the amplitude of the second peak is solution to

$$\frac{1}{4M_2\omega_2} \left[C_{22} a_2^2 + C_{12} \frac{\mathcal{F}_1^2}{\mu_1^2\omega_1^2} \right] \pm \sqrt{\frac{\mathcal{F}_2^2}{M_2^2\omega_2^2 a_2^2} - \frac{\mu_2^2}{M_2^2}} = 0, \quad (103)$$

which is a cubic equation for a_2^2 . Once the solution $a_2(\mathcal{F}_1, \mathcal{F}_2)$ is known, we can reinstate it in (98) and we obtain the frequency shift, $\sigma_1 = \Omega - \omega_1$ as

$$\sigma_1(\mathcal{F}_1, \mathcal{F}_2) = \frac{1}{4M_1\omega_1} \left[C_{11} \frac{\mathcal{F}_1^2}{\mu_1^2\omega_1^2} + C_{12} a_2^2(\mathcal{F}_1, \mathcal{F}_2) \right], \quad (104)$$

which provides the frequency shift as a function of the forces (or driving power), \mathcal{F}_1 and \mathcal{F}_2 , of the fundamental and excited modes.

V. CONCLUSION

Here, we have presented two analytical models that yield closed-form solutions describing the dynamics of the coupled-beam resonator, dubbed the antenna structure. This structure is a prototype of a class of two-element mechanical structures that can be envisioned in specific applications that involve coupled mechanical oscillators and hierarchical structures. The inherent modifications associated with the dynamics of coupled-element structures can be engineered to result in advantageous frequency and amplitude performance, which is otherwise difficult to obtain with simple geometries. In particular, the measurements of a similar nanomechanical fabricated device have been reported previously [12, 23] to demonstrate some of the highest mechanical resonance frequencies up to 3 GHz, reported to date.

The continuum model allows for a clear comparison of the modal shapes and spectrum with full finite element analysis of the structure. The findings and resulting discussion of Sec. III G elucidate the behavior of the coupled-element system in the fundamental and first collective modes. In particular, it is shown that the enhanced effective amplitude of the collective mode results from the collective excitation of the cantilever continuum at high frequencies, while the supporting central beam effectively adds the cantilever motion by moving in its fundamental mode shape with zero nodes, thus providing maximum transduction of the cantilever displacement to the measured magnetomotive voltage.

We have further investigated the driven damped model of the system as well as the nonlinear modal coupling between widely spaced modes of the structure using perturbation theory techniques. The results elucidate the response of experimentally measured structures that show modal interactions even in the limit of linear driving (to be published elsewhere). The analysis, however, is readily applied to a general set of coupled element weakly damped and weakly nonlinear resonators, and it illustrates the nontrivial modifications in the dynamics of such systems that can be carefully engineered to suit specific technical needs. As was mentioned in the section I, applications of RF MEMS and NEMS devices are numerous in the areas of wireless communications and frequency manipulation.

Acknowledgments

This work is supported by NSF (DMR-0449670).

APPENDIX A: GENERAL SOLUTION TO THE DISCRETE MODEL

The solution to the system of equations (12)-(13) reads

$$Y(u) = C_1^{(j)} \cos(\mu u) + C_2^{(j)} \sin(\mu u) + C_3^{(j)} \cosh(\mu u) + C_4^{(j)} \sinh(\mu u) \text{ for } u \in (u_{j-1}, u_j), \quad (\text{A1})$$

with $j \in \{1, \dots, N+1\}$, and

$$H_i(v) = [A_1(\gamma) \cos(\gamma v) + A_2(\gamma) \sin(\gamma v) + A_3(\gamma) \cosh(\gamma v) + A_4(\gamma) \sinh(\gamma v) - 1] Y(u_i), \quad (\text{A2})$$

with $i \in \{1, \dots, N\}$, $u_0 = 0$ and $u_{N+1} = 1$. Given the boundary conditions (14), we can solve for $A_j(\gamma)$ in Eq. (A2) and find the result given in Eq. (30). Now, let $C^{(j)} = (C_1^{(j)}, \dots, C_4^{(j)})^T$. Using the boundary conditions (14) for $Y(u)$ at u_j , we obtain [29]

$$C^{(j+1)} = (\mathbb{1} + 2\alpha A_2(\gamma) \mathbf{K}_j(\mu)) C^{(j)}, \quad j \in \{1, \dots, N\}, \quad (\text{A3})$$

where the quantities involved are defined in section II C. The boundary conditions Eq. (14) at $u = 0$ show that $C_3^{(1)} = -C_1^{(1)}$ and $C_4^{(1)} = -C_2^{(1)}$. The problem is then reduced to the two components $C_1^{(1)}$ and $C_2^{(1)}$. Rewriting them as the 2-vector $c^{(1)} = (C_1^{(1)}, C_2^{(1)})^T$, we have

$$C^{(1)} = \mathbf{L} c^{(1)}, \quad (\text{A4})$$

where \mathbf{L} is defined in Eq. (17). At the other end of the beam, $u = 1$, the boundary conditions can also be cast into a matrix form as

$$\mathbf{T}(\mu) C^{(N+1)} = 0, \quad (\text{A5})$$

where $\mathbf{T}(\mu)$ is again defined in Eq. (17). Putting Eqs. (A3), (A4) and (A5) together, we finally see that

$$\mathbf{M}(\omega) c^{(1)} = 0. \quad (\text{A6})$$

where the 2×2 matrix $\mathbf{M}(\omega)$ is given in (16). This system has a nonzero solution $c^{(1)}$ if and only if the determinant of $\mathbf{M}(\omega)$ is zero, hence the secular equation

$$\det \left(\mathbf{T}(\mu) \left[\prod_{j=1}^N (\mathbb{1} + 2\alpha A_2(\gamma) \mathbf{K}_j(\mu)) \right] \mathbf{L} \right) = 0. \quad (\text{A7})$$

Once a solution ω_n of (A7) has been found, the coefficients $C_i^{(j)}(\omega_n)$, $i = 1, \dots, 4$, of the corresponding mode, $Y_n(u)$, are automatically determined by Eqs. (A3) and (A6) as

$$C^{(j+1)}(\omega_n) = \left[\prod_{k=1}^j (\mathbb{1} + 2\alpha A_2(\gamma_n) \mathbf{K}_k(\mu_n)) \right] C^{(1)}(\omega_n), \quad (\text{A8})$$

with $j \in \{1, \dots, N\}$ and

$$C^{(1)}(\omega_n) = \mathbf{L} c^{(1)}(\omega_n) \text{ and } c^{(1)}(\omega_n) = \mathcal{N} \begin{pmatrix} M_{12}(\omega_n) \\ -M_{11}(\omega_n) \end{pmatrix}, \quad (\text{A9})$$

where M_{ij} are the coefficients of the matrix \mathbf{M} . Ultimately, the normalization factor \mathcal{N} is determined from $\int_0^1 Y_n(u)^2 du = 1$.

APPENDIX B: SOLUTION OF THE DISCRETE MODEL FOR $N = 1$ (TWO CANTILEVERS)

In this appendix, we find the solution of the discrete model for two cantilevers ($N = 1$) located on both sides of the beam in its middle and we briefly compare it to the solution of the continuum model with the same number of cantilevers. Using the general result provided in (A7), we can cast the secular equation into the form

$$\mathcal{A}(\mu) \mathcal{S}(\gamma, \mu) = 0, \quad (\text{B1})$$

where

$$\mathcal{A}(\mu) = \sin \frac{\mu}{2} \cosh \frac{\mu}{2} - \sinh \frac{\mu}{2} \cos \frac{\mu}{2} \quad (\text{B2})$$

and

$$\begin{aligned} \mathcal{S}(\gamma, \mu) = & 2\alpha A_2(\gamma) \left(\cos \frac{\mu}{2} \cosh \frac{\mu}{2} - 1 \right) + \\ & + \sin \frac{\mu}{2} \cosh \frac{\mu}{2} + \sinh \frac{\mu}{2} \cos \frac{\mu}{2}. \end{aligned} \quad (\text{B3})$$

where $A_2(\gamma)$ is given in (30) and $\alpha = w/W$. The factorization of the secular equation has a clear physical meaning. It is the result of the mirror symmetry of the problem with respect to the middle of the beam. Because of it, the modes of the discrete model are either symmetric (Y_s) or antisymmetric (Y_a) with respect to the latter. In what follows, we use Eqs. (A9) and (B1) to calculate the analytical form of the modal shape of the symmetric and antisymmetric modes for the central beam and the cantilevers.

1. Symmetric modes

Symmetric modes satisfy $Y_s(u) = Y_s(1-u)$. Their secular equation is given by ($\mu > 0, \gamma > 0$),

$$\mathcal{S}(\gamma, \mu) = 0, \quad (\text{B4})$$

where $\mathcal{S}(\gamma, \mu)$ is given in (B3) and, according to Eq. (11), $\mu = \gamma L/l$. The corresponding frequency is obtained from

$$\omega = \sqrt{\frac{\mathcal{E}_b}{\mu_b}} \left(\frac{\mu}{L} \right)^2 = \sqrt{\frac{\mathcal{E}_t}{\mu_t}} \left(\frac{\gamma}{l} \right)^2. \quad (\text{B5})$$

The expression for the modal shape of the central beam is,

$$Y_s(u) = \mathcal{N} \left\{ \cos(\mu u) - \cosh(\mu u) + \left(\frac{\sin \frac{\mu}{2} + \sinh \frac{\mu}{2}}{\cos \frac{\mu}{2} - \cosh \frac{\mu}{2}} \right) \times \right. \\ \left. \times (\sin(\mu u) - \sinh(\mu u)) \right\}, \quad u \in \left[0, \frac{1}{2} \right], \quad (\text{B6})$$

with a normalization factor \mathcal{N} given by

$$\mathcal{N} = \left[1 + \frac{6 (\cos \frac{\mu}{2} \cosh \frac{\mu}{2} - 1)}{\mu (\cos \frac{\mu}{2} - \cosh \frac{\mu}{2})^2} \times \right. \\ \left. \times (\cos \frac{\mu}{2} \sinh \frac{\mu}{2} + \cosh \frac{\mu}{2} \sin \frac{\mu}{2}) \right]^{-1/2}. \quad (\text{B7})$$

To evaluate the deflection of the cantilevers, we use Eq. (A2) and find

$$H_1(v) = [A_1(\gamma) \cos(\gamma v) + A_2(\gamma) \sin(\gamma v) + \\ + A_3(\gamma) \cosh(\gamma v) + A_4(\gamma) \sinh(\gamma v) - 1] Y_s(1/2), \quad (\text{B8})$$

where the coefficients A_i are given in Eq. (30) and where the deflection of the middle of the beam is determined from (B6) as

$$Y_s(1/2) = 2\mathcal{N} \left(\frac{1 - \cos \frac{\mu}{2} \cosh \frac{\mu}{2}}{\cos \frac{\mu}{2} - \cosh \frac{\mu}{2}} \right). \quad (\text{B9})$$

2. Antisymmetric modes

Antisymmetric modes satisfy $Y_a(1-u) = -Y_a(u)$, which leads to $Y_a(1/2) = 0$. The deflection of the cantilevers is then zero, $H_1(v) = 0$. In this case, we directly see from equations (12) and (14), that $Y_a(u)$ satisfies a simple clamped-clamped beam equation and that its third derivative has no discontinuity in $u = 1/2$, given that $H_1(v) = 0$. The shape of the antisymmetric modes is then similar to Eq. (33), which yields

$$Y_a(u) = \left\{ \cos(\mu u) - \cosh(\mu u) - \left(\frac{\cos \mu - \cosh \mu}{\sin \mu - \sinh \mu} \right) \times \right. \\ \left. \times (\sin(\mu u) - \sinh(\mu u)) \right\}, \quad u \in [0, 1]. \quad (\text{B10})$$

From Eq. (B1), we see that μ has to be a root of the secular equation

$$\mathcal{A}(\mu) = 0, \quad (\text{B11})$$

where $\mathcal{A}(\mu)$ is given in (B2). It turns out that Eq. (B11) is equivalent to the usual clamped-clamped secular equation, $\cos(\mu) \cosh(\mu) = 1$, provided it is restricted to antisymmetric modes. Indeed, $\cos(\mu) \cosh(\mu) = 1$ factorizes as $\mathcal{A}(\mu) \mathcal{A}^+(\mu) = 0$ where $\mathcal{A}^+(\mu) = \sin \mu/2 \cosh \mu/2 + \sinh \mu/2 \cos \mu/2$: $\mathcal{A}(\mu) = 0$ provides the frequencies of antisymmetric modes while $\mathcal{A}^+(\mu) = 0$ gives the frequencies of the symmetric modes of a simple clamped-clamped beam. When cantilevers are affixed to the middle of the

beam, symmetric modes are affected by their motion and the secular equation becomes $\mathcal{S}(\gamma, \mu) = 0$ (see Eq. (B4)) rather than $\mathcal{A}^+(\mu) = 0$. Their modal shape changes from (33) to (B6). For antisymmetric modes, however, the cantilevers do not move so that, modal shape and frequency remain unaffected.

The first roots of Eq. (B11) are given by $\mu \simeq 7.8532, 14.1371$, and $(2n+1/2)\pi$ as n becomes large. The corresponding frequencies are obtained from Eq. (B5). Notice that, in this particular case, the modal shape of an antisymmetric mode of the discrete model is exactly the same as the modal shape of the continuum model. Their frequency differs however. Even though μ and β (see Eq. (34)) satisfy the same secular equation (and are thus equal), the frequency of the continuum model is obtained by solving equation (32) whose solution, γ_c , is not proportional to β while the solution of the discrete model, γ_d , satisfies $\gamma_d = \mu l/L$. The frequencies, both obtained from Eq. (B5), are thus different. The exact similarity of the modes may seem surprising at first glance because, if the cantilevers are at rest in the discrete model and thus do not participate to the motion, in the continuum model, the force density of the cantilever has been spread all over the beam and, consequently, the cantilever continuum moves with the beam. Nonetheless, as the force density it generates is everywhere proportional to the mode shape $Y(u)$, the frequency is detuned but the mode shape remains as is.

3. Comparison with the continuum model

According to the dimensions of the antenna, $L/l \simeq 21.4$ and $w/W \simeq 0.5$. Then $\mu \simeq 21.4\gamma$ and $\alpha = 0.5$. Plugging these values into Eq. (B4), we can solve for γ_d and obtain the values for the symmetric modes reported in Table I, namely $\gamma_{d,1} = 0.2149$ and $\gamma_{d,3} = 0.5035$. For the antisymmetric modes, we use $\mu \simeq 21.4\gamma$ and the values quoted in the previous section and find $\gamma_{d,2} = 0.3670$ and $\gamma_{d,4} = 0.6606$. Now, solving equation (34) for $\beta = \beta_1$ to β_4 , where β_n are the successive roots of $\cos(\beta) \cosh(\beta) = 1$, we find the corresponding values of γ_c for the continuum model, reported in the third column of Table I. As we see, these values are very close to those of the discrete model. Using Eq. (B5) we finally report the frequencies of the discrete (4th column) and continuum (5th column) modes. Their relative frequency difference is displayed in the 6th column. The modal shapes of the beam and the cantilevers from the fundamental mode up to the third excited mode are depicted in Fig. 7. For the cantilever continuum, we have displayed the deflection at $u = 1/2$ only. As we can see, symmetric modes are very similar and antisymmetric modes are exactly the same.

Beside the first levels presented in table I, we have found numerically that the agreement between the spectra of the discrete and continuum models is very good in the sense that there is almost always one frequency of the continuum spectrum that closely matches the corresponding frequency of the discrete model. The shape of

TABLE I: Values for the parameters γ_d (discrete model) and γ_c (continuum model) derived from Eqs. (B4)-(B11) and (34), respectively. Frequencies are determined from Eq. (B5) for the antenna parameters given in the introduction. The symmetry class of the modes is denoted by s (symmetric) or a (antisymmetric).

Mode	Symmetry	γ_d	γ_c	f_d^a (MHz)	f_c^a (MHz)	$\Delta f/f$ (in %)
Fundamental	s	0.2149	0.2185	31.81	32.88	-3.25
First Excited	a	0.3670	0.3628	92.74	90.64	2.31
Second Excited	s	0.5035	0.5079	174.6	177.7	-1.74
Third Excited	a	0.6606	0.6530	300.5	293.4	2.33

^aThe frequency is determined as $f = \omega/2\pi$

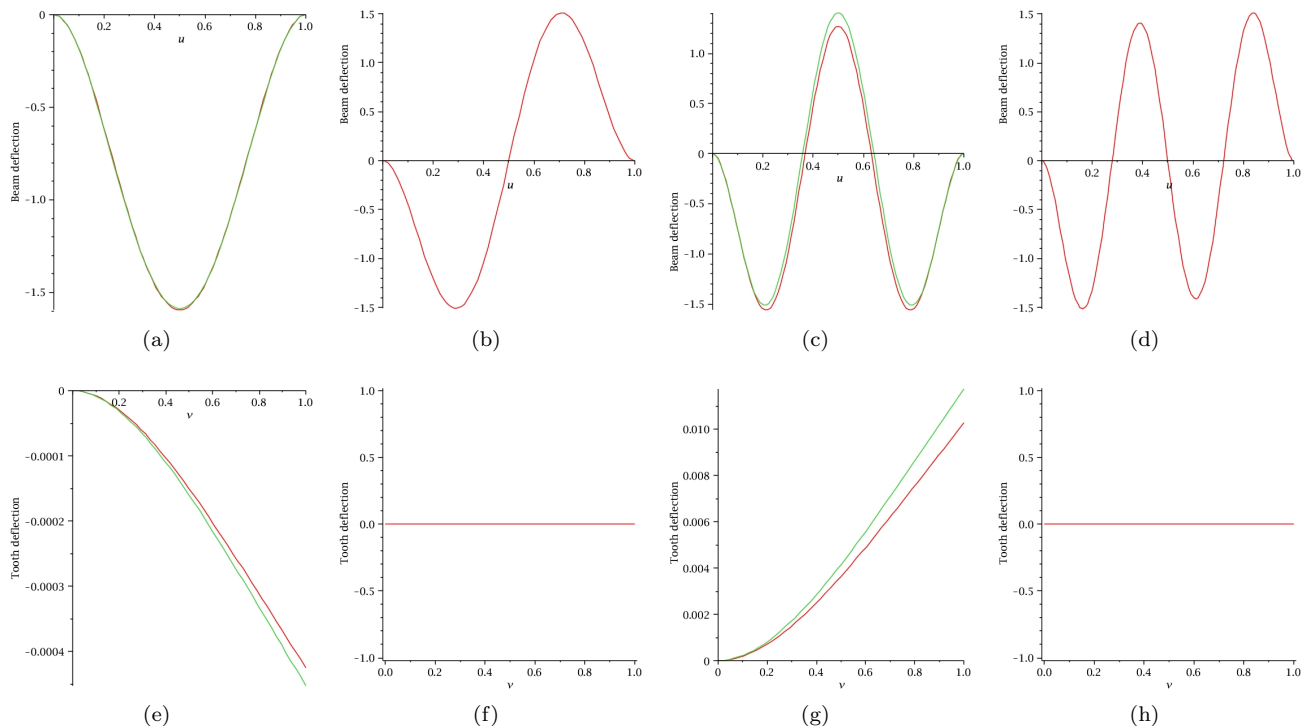


FIG. 7: Fundamental to third excited mode shapes of the central beam ((a),(b),(c),(d)) and of the cantilever ((e),(f),(g),(h)). The results of the discrete and continuum models are in red and green, respectively. For comparison, the deflection of the cantilever continuum is shown at $u = 1/2$ only. The antisymmetric discrete and continuum modes are exactly the same but their frequencies are different (see Table I).

the central beam is very similar (same n) for matching frequencies. The frequencies of the discrete model, however, are quite regularly spaced while in addition to producing these regularly spaced frequencies, the spectrum of the continuum model also forms clusters of nearly degenerate frequencies as explained in section III E. It is clear from the data we have obtained that, in the discrete model, the excitation level (n) of the central beam increases regularly with the frequency. In the continuum model, however, this excitation level increases from $n = 1$ to infinity within each band, that is from $\omega_{1,k}$ up to $\omega_{\infty,k}$ determined by Eq. (38). Therefore, the continuum frequencies that match the discrete ones are located *away* from the band edge clusters of the continuum spectrum. The continuum frequencies that accumulate close to the band edges have therefore no ($N = 1$) discrete equivalent. In other words, collective modes such as those observed

in the continuum model appear only when the number of cantilevers is large enough for the continuum approximation to hold.

APPENDIX C: ANALYTICAL AND NUMERICAL RESULTS FOR EQS. (93)

Using Eqs. (33) and (29), all the integrals involved in the calculation of the effective parameters of the time average Lagrangian, see Eq. (93), can normally be evaluated analytically. For Γ_i , $i \in \{1, \dots, 4\}$, results are simple

enough to be displayed below.

$$\begin{aligned}\Gamma_1 &= \frac{\beta_1 t}{2}(\beta_1 t + 2) \simeq 6.1513, \\ \Gamma_2 &= \frac{\beta_1^5 t}{10}(5\beta_1 t + 11) \simeq 2846.4975, \\ \Gamma_3 &= \frac{3}{4} \left(3 - t^4 - \frac{2t^3}{\beta_1} \right) \simeq 1.8519, \\ \Gamma_4 &= \frac{4t}{\beta_1} \simeq -0.8308\end{aligned}$$

where $t = \tan(\beta_1/2)$. Note that $\cos(\beta_1) = 1/\cosh(\beta_1)$ and $\sin(\beta_1) = -\tanh(\beta_1)$. Apart from $\Lambda_{ii} = L_{ii} - 2A_2(\gamma_i)/\gamma_i$ and $L_{ii} \equiv L(\gamma_{1,i})$, given in Eq. (51), the other integrals have been evaluated numerically for the parameters given in II A. We have found

$$\begin{aligned}L_{11} &\simeq 1.00012 ; L_{22} \simeq 3.89887, \\ \Lambda_{11} &\simeq 6.16 \times 10^{-5} ; \Lambda_{22} \simeq 4.9687, \\ I_{11} &\simeq 1.64 \times 10^{-16} ; I_{22} \simeq 232.49, \\ I_{12} &\simeq 1.94 \times 10^{-7} ; K_{1212} \simeq 8.26 \times 10^{-7}, \\ K_{1111} &\simeq 6.58 \times 10^{-16} ; K_{2222} \simeq 1.07 \times 10^3, \\ K_{1122} &\simeq 9.84 \times 10^{-7} ; K_{2211} \simeq 6.98 \times 10^{-7}.\end{aligned}$$

So that, finally,

$$\begin{aligned}M_1 &= 1.74 \times 10^{-14} ; M_2 = 4.17 \times 10^{-14}, \\ \mathcal{F}_i &= -4.44 \times 10^{-6} f_i ; C_{12} = 1.65 \times 10^{17}, \\ C_{11} &= -5.07 \times 10^{13} ; C_{22} = 1.05 \times 10^{21}, \\ \omega_1 &= 1.55 \times 10^8 ; \omega_2 = 1.85 \times 10^{10}.\end{aligned}$$

where all the results are given in SI units. From the quantities ω_j , the frequencies of the fundamental and collective modes are 24.7 MHz and 2.94 GHz, respectively.

-
- [1] J. A. Wheeler and W. H. Zurek, Quantum Theory and Measurement (Princeton University, Princeton, 1983).
- [2] W. Zurek, Rev. Mod. Phys. 75, 715 (2003).
- [3] I. Martin and W. H. Zurek, Phys. Rev. Lett. 98, 120401 (2007).
- [4] C. Caves et al., Rev. Mod. Phys. 52, 341 (1980).
- [5] M. Bocko and R. Onofrio, Rev. Mod. Phys. 68, 755 (1996).
- [6] H. J. Mamin and D. Rugar, Appl. Phys. Lett. 79, 3358 (2001).
- [7] D. Rugar, R. Budakian, H. J. Mamin, and B. W. Chui, Nature 430, 329 (2004).
- [8] J. Dornigac, A. Kalinowski, S. Erramilli, P. Mohanty, Phys. Rev. Lett. 96, 186105 (2006).
- [9] V. B. Braginsky and F. Y. Khalili, Rev. Mod. Phys. 68, 1 (1996).
- [10] C. Montemagno and G. Bachand, Nanotech. 10, 225 (1999).
- [11] G. Wu, H. Ji, K. Hansen, T. Thundat, R. Datar, R. Cote, M. Hagan, A. K. Chakraborty, and A. Majumdar, Trans. Nat. Acad. Sci. U.S.A. 98, 1560 (2001).
- [12] A. Gaidarzhy, G. Zolfagharkhani, R. L. Badzey, and P. Mohanty, Phys. Rev. Lett. 94, 030402 (2005).
- [13] M. D. LaHaye, O. Buu, B. Camarota, and K. C. Schwab, Science 304, 74 (2004).
- [14] P. Mohanty, to be published in Novel Nonlinear Devices (2008).
- [15] C. T. C. Nguyen, IEEE Trans. Microwave Theory Tech. 47, 1486 (1999).
- [16] C. T. C. Nguyen, L. P. B. Katehi, and G. M. Rebitz, Proc. IEEE 86, 1756 (1998).
- [17] R. Badzey, G. Zolfagharkhani, A. Gaidarzhy, and P. Mohanty, Appl. Phys. Lett. 85, 3587 (2004).
- [18] P. Mohanty, G. Zolfagharkhani, S. Kettermann, and P. Fulde, Phys. Rev. B 70, 195301 (2004).
- [19] R. Maranganti and P. Sharma, Phys. Rev. Lett. 98, 195504-4 (2007).
- [20] X. M. H. Huang, C. Zorman, M. Mehregany, and M. L. Roukes, Nature 421, 496 (2003).
- [21] A. Gaidarzhy, M. Imboden, P. Mohanty, B. Sheldon, and J. Ranken, Appl. Phys. Lett. 91, 203503 (2007).
- [22] F. D. Bannon III, J. R. Clark, and C. T.-C. Nguyen, IEEE J. Solid-State Cir. 35, 512526 (2000).
- [23] A. Gaidarzhy, G. Zolfagharkhani, R. Badzey, and P. Mohanty, Appl. Phys. Lett. 86, 254103 (2005).
- [24] Clarence V. de Silva, Vibration: fundamentals and practice, CRC Press, Taylor and Francis Group, second edition (2007), p. 385-439.
- [25] Lee A. Segel, Mathematics Applied to Continuum Mechanics, Dover Publications, Inc., New York (1987), p. 207.
- [26] James M. Gere, Stephen P. Timoshenko, Mechanics of materials, Boston : PWS Pub Co. (1997).
- [27] A.H. Nayfeh, P.F. Pai, Linear and Nonlinear Structural Mechanics, Wiley series in nonlinear science, Wiley-Interscience (2004).
- [28] A. Gaidarzhy, Resonant Nanomechanical Motion at Gigahertz Frequencies, Ph.D. Thesis, Boston University (2007).
- [29] Because of Eqs. (A2) and (30), we have $Y'''(u_j^+) - Y'''(u_j^-) = -RH_j'''(0) = 2\gamma^3 R A_2(\gamma) Y(u_j) = 4\mu^3 \alpha A_2(\gamma) Y(u_j)$, where $\alpha = w/W$.